Surface-mediated Bacteriophage Defense Incurs Fitness Tradeoffs for Interbacterial Antagonism

Chia-En Tsai[1,2,5], Feng-Qi Wang[2,5], Chih-Wen Yang[3], Ling-Li Yang[2], Yung-Chih Chen[2], Po-Yin Chen[1,2], Ing-Shouh Hwang[3], See-Yeun Ting[1,2,4†]

[1] Molecular and Cell Biology, Taiwan International Graduate Program, Academia Sinica and National Defense Medical Center, Taipei, 11490, Taiwan

[2] Institute of Molecular Biology, Academia Sinica, Taipei 11529, Taiwan

[3] Institute of Physics, Academia Sinica, Taipei 115201, Taiwan

[4] Genome and Systems Biology Degree Program, National Taiwan University, Taipei 106319, Taiwan

[5] These authors contributed equally

[†]Correspondence: syting@gate.sinica.edu.tw

Keywords:

Phage; Lipopolysaccharide; Interbacterial Antagonism; Bacterial Immunity; Tail Spike Protein

ABSTRACT

Bacteria in polymicrobial habitats are constantly exposed to biotic threats from bacteriophages, antagonistic bacteria, and predatory eukaryotes. These antagonistic interactions play crucial roles in shaping the evolution and physiology of bacteria. To survive, bacteria have evolved mechanisms to protect themselves from such attacks, but the fitness costs of resisting one threat and rendering bacteria susceptible to others remain unappreciated. Here, we examined the fitness consequences of bacteriophage resistance in *Salmonella enterica*, revealing that phage-resistant variants exhibited significant fitness loss upon co-culture with competitor bacteria. These phage-resistant strains display varying degrees of lipopolysaccharide (LPS) deficiency and increased susceptibility to contact-dependent interbacterial antagonism, such as the type VI secretion system (T6SS). Utilizing mutational analyses and atomic force microscopy, we show that the long-modal length O-antigen of LPS serves as a protective barrier against T6SS-mediated intoxication. Notably, this competitive disadvantage can also be triggered independently by phages possessing LPS-targeting endoglycosidase in their tail spike proteins, which actively cleave the O-antigen upon infection. Our findings reveal two distinct mechanisms of phage-mediated LPS modifications that modulate interbacterial competition, shedding light on the dynamic microbial interplay within mixed populations.

INTRODUCTION

Microbial communities are frequently subjected to antagonistic interactions within their environments, predominantly from bacteriophages, bacterial competitors, and unicellular predatory eukaryotes. Phages, the most abundant biological entities on Earth, possess the capacity to devastate entire bacterial populations through lytic cycles[1]. Similarly, bacterial competitors

44 employ a diverse array of specialized mechanisms, such as the production of antibiotics, secretion
45 of antimicrobial peptides, deployment of toxin delivery systems, and utilization of membrane-
46 puncturing nanomachines, all aimed at inhibiting or killing rival bacteria[2-5]. Moreover, unicellular
47 eukaryotic predators, such as free-living protozoa, exert predation pressure on bacterial
48 populations through phagocytosis[6]. Collectively, these antagonistic interactions impose significant
49 selective pressures on bacteria that profoundly influence their evolution, ecology, and physiology.

50 To survive in such hostile environments, bacteria have evolved a broad spectrum of defense
51 mechanisms against biotic threats[7]. To mitigate or evade phage infection, bacteria have developed
52 strategies targeting nearly every stage of the phage life cycle[8]. Extracellular defenses, including
53 mutations or downregulation of surface receptors (*e.g.,* membrane proteins and
54 lipopolysaccharides), can prevent phage attachment and subsequent infection[9, 10]. Intracellularly,
55 widely distributed defense systems—such as restriction-modification systems, CRISPR-Cas
56 systems, and abortive infection mechanisms, act to neutralize phages post-entry[8, 11, 12]. Parallel to
57 these antiviral defenses, bacteria have also evolved strategies to counteract the antagonism posed
58 by competitor bacteria. For instance, the acquisition of immunity determinants endows resistance
59 against specific interbacterial toxins and antimicrobial compounds[13, 14]. Furthermore, general
60 stress responses and competition-sensing pathways enhance bacterial resilience to antimicrobial
61 agents in both environmental and clinical contexts[15-17]. This dynamic interplay between microbial
62 offense and defense underscores the central importance of these interactions in shaping microbial
63 communities.

64 Although biotic pressures imposed by other microbes significantly drive the evolution of
65 bacterial immunity, accumulating evidence indicates that this evolutionary process is frequently
66 associated with fitness trade-offs[18]. A prominent example is bacterial surface modifications that

67 hinder phage attachment but concurrently compromise bacterial fitness upon encountering
68 antibiotics or host immune systems[10, 19-21]. Similarly, CRISPR-Cas immunity has been shown to
69 impose an increased metabolic burden on host cells, which may limit its distribution across
70 bacterial taxa[22-25]. Furthermore, though a mucoid phenotype confers partial protection against
71 bacteriophage infection, it often incurs fitness costs in the context of bacterial competition[26-28].
72 Recent research on *Escherichia coli* has also demonstrated that genetic variants resistant to
73 interbacterial intoxication may suffer from growth defects and increased susceptibility to
74 antimicrobial agents and environmental stresses[29]. Such fitness trade-offs associated with
75 antagonistic coevolution are highly context-dependent[30], but predicting their impact on microbial
76 community composition remains challenging due to the mechanisms underlying these fitness costs
77 frequently being poorly characterized.

78 In this study, we report that though bacteria develop surface modifications to protect
79 against viral infection, these modifications result in significant trade-offs in interbacterial
80 competition with antagonistic bacteria. We provide evidence that lipopolysaccharide (LPS), a
81 major component of the bacterial outer membrane, plays a previously unappreciated role in
82 protecting against contact-dependent killing by bacterial competitors. Remarkably, we have
83 discovered that mutations in LPS biosynthesis genes, as well as interactions with phages encoding
84 LPS-targeting endoglycosidase in their tail spike proteins, contribute to the observed competitive
85 disadvantage. Our study identifies two distinct mechanisms by which phage-mediated LPS
86 modifications influence interbacterial competition, highlighting the role of antagonistic
87 coevolution in shaping bacterial composition within polymicrobial communities.

88

89 **RESULTS**

90 **Phage-resistant *S. enterica* Displays Competitive Fitness Deficits in Co-culture with Bacterial**
91 **Competitors**

92 To investigate if phage-resistant bacteria incur fitness consequences when interacting with
93 bacterial competitors, we began by obtaining phage-resistant variants of the model bacterium,
94 *Salmonella enterica* serovar Typhimurium, from an established transposon insertion library for
95 pairwise bacterial co-culture experiments[31, 32] (Figure 1a). We reasoned that using this model
96 bacterium and the mutant library would facilitate the identification of underlying pathways
97 associated with competitive fitness costs. Consequently, we isolated distinct *S. enterica* variants
98 that were resistant to model phages from different families of Caudovirales: Felix O1
99 (Myoviridae)[33], P22 (Podoviridae)[34], and Chi (Siphoviridae)[35] (Supplementary Figure 1a, b).
100 Mutants exhibiting no significant growth defects under standard conditions were selected for
101 further analysis (Supplementary Figures 1c, d). We then co-cultured individual strains with
102 competitor bacteria, *i.e.*, Enterohemorrhagic *Escherichia coli* (EHEC) or *Enterobacter cloacae,* in
103 a one-to-one ratio in both liquid and solid media. We selected EHEC and *E. cloacae* due to their
104 ecological overlap with *S. enterica* in the mammalian gastrointestinal tract, where they frequently
105 co-occur during infections, representing a relevant model for studying competitive interactions in
106 both environmental and clinical contexts[36-38].

107 Compared to the wild-type *S. enterica* strain, we found that none of the phage-resistant
108 mutants exhibited competitive fitness differences in liquid broth co-culture assays with EHEC or
109 *E. cloacae* (Figure 1b). However, in solid media, though phage-resistant mutants exhibited no
110 observable fitness cost when incubated with EHEC, strains resistant to the Felix O1 and P22
111 phages displayed significant competitive disadvantage (relative survival < 1) upon co-cultured
112 with *E. cloacae* (Figure 1c). This competitive phenotype was restricted to solid media, where cell-

113 cell contacts are relatively stable, indicating that the stress imposed by *E. cloacae* is likely contact-
114 dependent[39]. Interestingly, resistant strains against phage Chi did not present a similar fitness
115 disadvantage, indicating that bacteriophage-specific resistance mechanisms might underlie the
116 competitive trade-offs in *S. enterica* (Figure 1c). These findings prompted us to prioritize
117 investigating: (1) which gene mutations in *S. enterica* conferring resistance to phages Felix O1 and
118 P22 impose interbacterial competitive disadvantages on the bacteria; and (2) what mechanism in
119 *E. cloacae* is critical for the competitive phenotype observed in our co-culture assay.
120

121 **Mutations in LPS Biosynthesis Genes Confer Competitive Disadvantages on *S. enterica***

122 To escape viral infection, bacteria often evolve and modify their surface receptors to
123 prevent phage entry[40]. Previous studies have identified LPS on the outer bacterial membrane as
124 the primary receptor for phages Felix O1 and P22[41, 42]. Accordingly, we postulated that our phage-
125 resistant *S. enterica* strains likely harbor mutations in LPS-related genes, thereby influencing their
126 susceptibility to *E. cloacae*. Indeed, we identified disruptive transposon insertions concentrated in
127 genes associated with the LPS biosynthesis pathway in our phage-resistant strains, indicating an
128 impairment in the outer membrane cell envelope of these mutants (Supplementary Figures 2a, b).
129 To confirm this finding, we compared LPS levels in these mutants relative to the wild-type strain.
130 LPS PAGE profiles revealed a significant reduction in LPS levels, particularly of the O-antigen,
131 in the Felix O1- and P22-resistant strains compared to wild-type (Figures 2a, b). In contrast, the
132 phage Chi-resistant *S. enterica* variants had transposon insertions in genes unrelated to LPS
133 biosynthesis, and their LPS levels were comparable to wild-type bacteria (Supplementary Figures
134 2c, d). Additionally, many of the Felix O1- and P22-resistant strains exhibited auto-aggregation in
135 unicellular culture (Supplementary Figures 2e, f), a phenotype associated with LPS deficiency[43,

136 [44]. These findings indicate that disruption of LPS biosynthesis genes contributes to the competitive
137 fitness defects observed in *S. enterica* co-cultured with *E. cloacae* (Figure 1c).
138
139 **Phage-resistant *S. enterica* Strains are More Susceptible to T6SS-mediated Intoxication**
140 Next, we sought to elucidate the underlying cell contact-dependent mechanisms utilized by
141 *E. cloacae* in competing with *S. enterica*. Prior studies have shown that *E. cloacae* relies on
142 functional secretory systems, such as the type VI secretion system (T6SS) and the contact-
143 dependent growth inhibition (CDI) pathway, to outcompete their bacterial rivals[45, 46]. These
144 secretory systems translocate antibacterial toxins into neighboring cells upon direct cell-cell
145 interaction, facilitating potent mechanisms of contact-dependent intoxication between bacteria[47,
146 48]. Therefore, we hypothesized that the competitive fitness trade-offs observed in the phage-
147 resistant strains might be attributable to interbacterial antagonism mediated by these secretory
148 systems.
149 To determine if such antagonistic pathways in *E. cloacae* contribute to the competitive
150 defects of the Felix O1- and P22-resistant *S. enterica* strains, we subjected them to pairwise
151 competition under contact-promoting conditions against *E. cloacae* mutant strains in which the
152 T6SS (Δ*tssM*) or CDI (Δ*cdiA*) had been inactivated[45, 46]. Consistent with our co-culture
153 experiments, the phage-resistant variants displayed reduced competitiveness when incubated with
154 wild-type *E. cloacae* (Figures 2c, d). Notably, T6SS inactivation abrogated the competitive defect
155 of the phage-resistant strains, whereas the competitive phenotype persisted in competition with *E.*
156 *cloacae* Δ*cdiA* (Figures 2e-h). These results support the notion that the competitive fitness deficit
157 in the phage-resistant strains arises from T6SS-mediated interbacterial antagonism.
158

159 **LPS O-antigen Protects *S. enterica* from T6SS-mediated Assaults**

160 Although the T6SS is an effective antibacterial mechanism, target cells can evade being
161 killed by avoiding direct contact with T6+ bacteria[49]. One strategy to do so is for target cells to
162 produce extracellular biopolymers, such as secreted exopolysaccharides, membrane-attached
163 capsules, or colanic acid, all of which may act as a physical barrier against T6SS-mediated
164 attacks[15, 50, 51]. LPS, a major component of Gram-negative bacterial surfaces, is known to confer
165 protection against external stresses such as antibiotics, antimicrobial peptides, and host immune
166 systems[52, 53]. Therefore, the observed competitive disadvantage we observed in LPS-deficient *S.*
167 *enterica* led us to explore the function of LPS in protecting against T6SS-mediated assaults.

168 LPS is comprised of lipid A covalently linked to core oligosaccharides (core OS) and
169 repetitive O-units (O-antigen) (Figure 3a). First, we sought to determine if the sugar composition
170 of the core OS is involved in protecting *S. enterica* against T6SS. We constructed in-frame
171 deletions of LPS-related genes in *S. enterica* differing in core OS structures (*i.e.,* WaaL, WaaJ,
172 WaaO, WaaG for the main chain OS structure, or WaaK, WaaB, WaaQ, WaaY for the side chain)[54]
173 (Figure 3a). If the LPS structure exerts a protective role, we anticipated that mutants hosting these
174 mutated genes would exhibit competitive fitness defects upon co-incubation with *E. cloacae*
175 carrying an active T6SS. Indeed, though mutations in the LPS-related genes did not result in
176 significant growth defects in unicellular cultures (Supplementary Figures 3a-c), strains deficient
177 in the genes essential for building the main chain OS structure displayed lower interbacterial
178 competitiveness than the wild-type strain (Figures 3b, c and Supplementary Figure 3d), similar to
179 the results we observed for LPS-deficient phage-resistant variants (Figures 2c, d). In contrast, *S.*
180 *enterica* mutants in which the side chain OS structure was perturbed presented indistinguishable
181 competitiveness to wild-type, except for the WaaK-deficient strain (Figures 3d, e and

182 Supplementary Figure 3e). Previous studies demonstrated that WaaK is required for proper ligation
183 of O-antigen to the core OS of LPS[55]. Indeed, LPS PAGE profiles supported the findings that O-
184 antigen levels in the Δ*waaK* strain were reduced significantly, *i.e.*, to levels similar to those in the
185 O-antigen ligase-knockout cells (Δ*waaL*) (Figure 3e). Together, these results indicate that the O-
186 antigen extending from the core OS plays a crucial role in protecting *S. enterica* from T6SS-
187 mediated interbacterial antagonism.

188 O-antigens are hypervariable repeat polysaccharides that present heterogeneity and a wide
189 range of chain lengths, which determine the uniqueness of bacterial serotypes[56]. Previous studies
190 have demonstrated that chain length regulators, such as WzzB and FepE, determine O-antigen
191 length and degree of polymerization in *S. enterica*[57, 58]. LPS PAGE profiles indicated that WzzB
192 is responsible for producing long (L)-modal length O-antigen chains (16-35 sugar repeat units),
193 whereas FepE is responsible for very long (VL) ones (>100 sugar repeat units) (Figure 3f). To
194 better define the protective role of O-antigen in protecting against interbacterial antagonism, we
195 constructed Δ*wzzB* and Δ*fepE* strains and subjected them to competition assays against *E. cloacae*
196 carrying an active T6SS. Interestingly, only the Δ*wzzB* cells displayed significant competitive
197 defects, whereas Δ*fepE* cells showed wild-type levels of protection (Figure 3g). In addition, both
198 mutants showed comparable survival in competition with *E. cloacae* Δ*tssM* (Supplementary Figure
199 3f). Therefore, our mutational analyses and LPS PAGE profiles indicated that L-modal length O-
200 antigen is sufficient to protect *S. enterica* from T6SS intoxication.

201

202 **LPS-mediated Protection Against T6SS Attack Extends to Other Gram-negative Bacteria**

203 Though LPS structure varies among Gram-negative species[56, 59], we speculated that its
204 intrinsic protective capacity against T6SS could be broadly conserved. We tested this hypothesis

205 by examining the protective function of LPS from the distantly related model species:
206 Enterohemorrhagic *E. coli* (EHEC) and *Citrobacter rodentium*. We constructed LPS-deficient
207 strains (Δ*waaO*) of these species and then subjected them to pairwise competition assays against
208 *E. cloacae* with or without an active T6SS. Compared to the wild-type strain, LPS-deficient cells
209 presented significant competitive deficits when incubated with *E. cloacae* carrying a functional
210 T6SS (Figures 3h, i). Inactivation of the T6SS abrogated the fitness defects of those variants in the
211 competition assay, supporting the notion that LPS-mediated protection against the T6SS is
212 conserved beyond *S. enterica* (Supplementary Figure 3g).
213

214 **LPS-targeting Endoglycosidase in Phage Tail Spike Protein Increases Susceptibility to**
215 **Interbacterial Antagonism**

216 We have demonstrated herein that mutations in *S. enterica* genes involved in LPS
217 biosynthesis lead to increased susceptibility to T6SS-mediated attacks. Nevertheless, apart from
218 genetic variations in bacteria altering LPS structures, external stresses can also induce LPS
219 modifications, thereby compromising their protective capacity against antimicrobials from
220 predators and hosts, as well as environmental factors[60]. Consequently, we wanted to examine if
221 external stress-mediated LPS modification could influence the susceptibility of *S. enterica* during
222 interbacterial competition.

223 In our investigation into potential external modifiers of LPS, we found that many phages,
224 including our model phage P22, encode a dual-function tail spike protein (TSP) with LPS-targeting
225 endoglycosidase activity[61] (Figure 4a, Supplementary Figure 1a). This phage protein mediates
226 recognition of the bacterial host LPS receptor and hydrolyzes the O-antigen, allowing phages to
227 penetrate the bacterial cell envelope and inject their DNA upon viral infection[41, 62] (Figures 4b, c).

228 Notably, the TSP is highly active and stable under extreme conditions, making it an ideal external
229 agent to test our hypothesis without genetically manipulating *S. enterica*[63].

230 Consistent with previous reports, the TSP from phage P22 could be heterologously
231 expressed and affinity-purified in high amounts[64] (Supplementary Figure 4a). LPS PAGE profiles
232 indicated that wild-type TSP, but not the catalytic aspartate mutant TSP_{D392N}, degraded the O-
233 antigen of *S. enterica* (Figure 4d). Cells treated with TSP (wild-type or D392N) did not exhibit
234 detectable growth defects in monoculture (Supplementary Figure 4b), but phage titers were
235 dramatically reduced, indicating that TSP treatment prevents P22 from recognizing the LPS
236 receptor (Figure 4e). Next, we assessed if TSP-treated *S. enterica* exhibits increased susceptibility
237 to T6SS-mediated assaults. Indeed, TSP-treated cells showed reduced interbacterial
238 competitiveness when co-incubated with *E. cloacae* possessing an active T6SS compared to the
239 control experiment using either wild-type cells or cells treated with TSP_{D392N} (Figure 4f). The
240 resulting competitive fitness defect was similar to that observed for the LPS-deficient strain
241 (Δ*waaL*) (Figure 4f). Inactivation of the T6SS abrogated the fitness defects in TSP-treated cells
242 (Figure 4g). These results indicate that external LPS modifiers from phages, such as TSP with
243 endoglycosidase activity, can sensitize *S. enterica* to T6SS-mediated attacks.

244

245 **Phage-carrying Endoglycosidase Sensitizes *S. enterica* to Interbacterial Antagonism in**
246 **Mixed Populations**

247 Our data to this point support a model whereby the endoglycosidase activity of TSP cleaves
248 LPS O-antigen on bacterial cell surfaces, thereby sensitizing the bacteria to T6SS-mediated
249 assaults (Figure 4f, g). However, treating cells with concentrated, purified TSP might yield non-
250 physiologically relevant outcomes. In natural polymicrobial communities, TSP is anchored to the

251 phage tail baseplate during viral particle assembly[65], so the free-form of TSP is likely present at
252 much lower concentrations than those used in our assays. Therefore, we investigated if the
253 presence of intact phage virions containing enzymatically active TSP could sensitize target bacteria
254 to interbacterial antagonism (Figure 5a).

255 Remarkably, when we incubated *S. enterica* with both phage P22 and *E. cloacae* carrying
256 an active T6SS, *S. enterica* survival significantly decreased (Figure 5b). The deficient fitness
257 phenotype was abolished when the T6SS of *E. cloacae* was inactivated or when *S. enterica* was
258 incubated with Felix O1 or Chi phages, which lack endoglycosidase activity in their tail spikes or
259 tail fibers[33, 66] (Figures 5b, c). These results corroborate our hypothesis that phages containing an
260 endoglycosidase targeting LPS sensitize host bacteria to T6SS-mediated attacks in mixed
261 microbial populations.

262 To validate this finding, we first ensured that *S. enterica* did not develop resistance to P22
263 during the phage-bacterium co-culture assay. Reinfecting surviving *S. enterica* with P22 resulted
264 in plaque titers comparable to those before the experiment, indicating that the competitive
265 phenotype was unlikely due to genetic adaptation (Supplementary Figure 5a). Next, we confirmed
266 that P22 does not cross-infect *E. cloacae*, as revealed by no P22 plaques being observed even at a
267 high plaque-forming unit (PFU) concentration using *E. cloacae* as the host (Supplementary Figure
268 5b). To further minimize the impact of viral infection from different phages, we subjected phages
269 to 254 nm UV-C irradiation to crosslink their DNA, preventing DNA injection into *S. enterica*
270 while retaining the enzymatic activity of TSP in the tail spikes (Figure 5d). Strikingly, though
271 phage titers decreased dramatically following UV treatment, the competitive fitness deficits
272 against the T6SS persisted in assays with *E. cloacae* and UV-treated P22 (Figures 5e-g). Again, no
273 detectable competitive fitness differences were observed when *S. enterica* was incubated with UV-

274 treated Felix O1 or Chi (Figures 5f, g and Supplementary Figures 5c, d). Together, these outcomes
275 strongly indicate that bacteriophages with endoglycosidase activity in their TSPs for binding and
276 hydrolyzing LPS increase the susceptibility of *S. enterica* to interbacterial antagonism in mixed
277 microbial populations.
278
279 **Evidence that the O-antigen of LPS Serves as a Physical Barrier against Interacting Bacteria**
280 The LPS-containing outer membrane of Gram-negative species serves as a barrier against
281 various harmful agents, including hydrophobic antibiotics, antimicrobial peptides, detergents, and
282 bile acids[67, 68]. The structural complexity of LPS is critical for regulating membrane permeability,
283 which may be compromised by any modifications[69]. Previous studies have demonstrated that LPS
284 remodeling can alter the negative charge on the bacterial surface or affect the binding of divalent
285 cations, thereby impacting the stability of the outer membrane[70]. Therefore, one plausible
286 explanation for the observed interbacterial competitive defects displayed by our LPS O-antigen-
287 deficient variants is an increase in permeability of their outer membrane. To investigate this
288 possibility, we performed two standard outer membrane permeability assays: *i*) N-phenyl-1-
289 napthylamine (NPN) uptake; and *ii*) vancomycin (VAN) sensitivity. NPN is a hydrophobic
290 fluorescent probe that exhibits increased fluorescence upon interacting with the hydrophobic core
291 of a disrupted membrane, making it a reliable indicator of membrane permeability[71]. Vancomycin,
292 a glycopeptide antibiotic, is typically ineffective against Gram-negative bacteria due to its large
293 molecular size and inability to penetrate an intact outer membrane. However, its efficacy can
294 increase if membrane integrity is compromised[72]. Therefore, these assays can provide robust
295 measures of outer membrane permeability.

296 In the NPN uptake assay, we observed that wild-type cells pretreated with the metal
297 chelator ethylenediaminetetraacetic acid (EDTA) showed a significant increase in NPN
298 fluorescence, indicative of membrane disruption. However, no significant difference in NPN
299 uptake was observed between the wild-type cells and the O-antigen-deficient mutants (*i.e.,* Δ*wzzB*,
300 which lacks L-modal length O-antigen, and Δ*waaL* that lacks all O-antigens) (Figure 6a). Similarly,
301 in the VAN sensitivity assay, neither mutant strain demonstrated increased sensitivity to
302 vancomycin compared to the wild-type strain (Figure 6b). These results are in line with previous
303 studies on LPS in *E. coli*, which have shown that the core OS of LPS is particularly crucial for
304 maintaining outer membrane permeability[73]. As both the Δ*wzzB* and Δ*waaL* mutants preserve the
305 core OS structure, their increased susceptibility to T6SS-mediated attacks is unlikely to be
306 attributable to compromised outer membrane permeability.

307 Given that the T6SS punctures and injects toxins into interacting bacteria in a contact-
308 dependent manner[74], we next hypothesized that the O-antigen of LPS might act as a physical
309 barrier, partially hindering T6SS-mediated penetration by limiting close-range interaction. To test
310 this hypothesis, we immobilized *S. enterica* wild-type and O-antigen-deficient mutants on a mica
311 substrate and employed atomic force microscopy (AFM) to characterize bacterial surface
312 morphology[75] (Figure 6c). Interestingly, the resolved AFM images reveal distinct and clear
313 grooved structures on the surfaces of both the wild-type and Δ*wzzB* mutant (Figures 6d, e). In
314 contrast, the Δ*waaL* mutant, which retains only the core OS, displayed a more flattened surface
315 (Figure 6f). A similar groove-like surface morphology has been observed in other bacteria[76, 77], and
316 flattened cell surfaces have been noted in O-antigen-deficient cells[78].

317 To gain more insight into the mechanical properties of LPS, we further analyzed the force-
318 distance curves, which represent the interaction between the AFM tip and the bacterial surface

319 (Figure 6g). The force-distance profiles of both wild-type and mutant strains exhibited two distinct
320 force-slope changes, indicative of interactions with two different substrates (Supplementary Figure
321 6). The first substrate corresponds to the LPS layer, and the second stiffer substrate represents the
322 outer membrane and cell wall (Figure 6c). For a more precise description, we defined point 1 as
323 the initial contact between the AFM tip and the LPS layer (x = 0, y = 0), and point 2 as the transition
324 point between the LPS layer and the outer membrane (Figure 6g). By measuring the distance
325 between points 1 and 2, we determined that LPS length in wild-type cells is 5.39±1.16 nm,
326 consistent with predictions for intact LPS structures (Figure 6h). In contrast, Δ*wzzB* cells, which
327 lack L-modal O-antigen, exhibited a reduced LPS length of 3.96±0.424 nm, and Δ*waaL* cells that
328 retain only the core OS had an LPS length of 3.39±0.41 nm (Figures 6i, j). LPS length in wild-
329 type cells was significantly more variable than in the mutants, implying heterogeneity in LPS
330 structure (Figure 6k). The loss of L-modal O-antigen in Δ*wzzB* led to a marked reduction in the
331 force region, similar to the reduction observed in the Δ*waaL* mutant (Figure 6k). These LPS lengths
332 are comparable to those reported in studies of *E. coli* strains with the core OS but lacking O-antigen,
333 for which LPS length was approximately 3±2 nm[76]. The reduction in LPS length we determined
334 for our O-antigen-deficient mutants indicates that the O-antigen functions as a physical barrier,
335 potentially hindering close interactions with competing bacteria.
336

337 **DISCUSSION**

338 Bacterial integrity has been shaped over billions of years through interactions with other
339 microorganisms, with antagonistic interactions serving as a key driver of bacterial evolution and
340 physiology[7]. Extensive research has elucidated the diverse mechanisms bacteria employ to defend
341 themselves from biotic threats, highlighting their importance in the survival and adaptation of

342 bacterial species. Although these defensive adaptations offer clear evolutionary benefits, they are
343 not without fitness costs[18, 25]. Our results demonstrate that though modification of surface receptors
344 enables bacterial populations to effectively resist and adapt rapidly to phage infection, such
345 adaptation imposes significant fitness costs, increasing susceptibility to contact-dependent killing
346 by other antagonistic bacteria. These findings emphasize the fine balance between adaptation and
347 vulnerability in microbial interactions, suggesting that antagonistic coevolution plays a pivotal role
348 in shaping the dynamics of bacterial communities.

349 Our results reveal a hitherto unappreciated dual role for LPS as both a receptor for phage
350 adsorption and a protective barrier against close-contact bacterial competitors. Our observation
351 that T6SS-mediated interbacterial antagonism is more effective against LPS-deficient strains
352 implies a significant evolutionary trade-off, wherein resistance to phage predation may increase
353 susceptibility to other biotic threats. Furthermore, our results indicate that the protective function
354 of LPS against the T6SS is likely conserved across different Gram-negative bacteria, as evidenced
355 by the similar competitive fitness defects observed in LPS-deficient variants of *E. coli* and *C.*
356 *rodentium*. This evolutionary conservation points to broader ecological implications, with
357 modifications of the LPS potentially significantly influencing microbial community composition
358 across different populations.

359 The extent to which LPS protects against other contact-dependent killing mechanisms
360 beyond the T6SS remains unclear. For example, bacterial genera such as *Xanthomonas* and
361 *Stenotrophomonas* possess a Type IV Secretion System (T4SS) specialized in transferring toxic
362 effectors into neighboring cells in a contact-dependent manner, leading to cell death[79-81]. The
363 evidence presented in our study supports that LPS functions as a physical barrier, potentially
364 hindering close contact with interacting bacteria. Therefore, it is plausible that LPS might similarly

365 interfere with toxin delivery by other bacterial nanomachines, representing a broader defensive
366 strategy against diverse biotic threats.

367 Interestingly, our study has also revealed that phages can influence interbacterial
368 competition in ways beyond direct lysis. Specifically, phages with endoglycosidase activity in their
369 TSPs can degrade the O-antigen of target bacteria, thereby sensitizing them to interbacterial
370 antagonism. This scenario adds a new dimension to our understanding of phage-bacterial
371 interactions, whereby phages not only act as predators but also modulate bacterial interactions by
372 compromising the structural integrity of bacterial membranes. Notably, purified TSP, unlike whole
373 phage particles, do not promote resistant mutations as they do not directly kill bacteria[82]
374 (Supplementary Figure 4b). Our discovery reveals a plausible mechanism by which TSP facilitates
375 the clearance of target cells, with antagonistic bacteria that occupy the same ecological niches
376 potentially eliminating competitors more effectively when the LPS of those competitors is cleaved
377 by exogenous TSP[64].

378 We propose a working model of how phages may act as a key modulator of interbacterial
379 competition within bacterial communities (Figure 7). In the absence of phages, bacterial
380 competitors deploy specialized weaponry, such as the T6SS, to antagonize rivals and promote
381 niche partitioning. However, in the presence of phages, two distinct scenarios could alter this
382 dynamic: (1) bacteria may develop protective modifications on their surfaces to prevent phage
383 adsorption, reducing the likelihood of infection; or (2) phages equipped with LPS-targeting
384 endoglycosidases in their TSPs cleave the LPS of recipient cells. Both scenarios increase the
385 susceptibility of target cells to contact-dependent killing, facilitating niche invasion and leading to
386 the competitive exclusion of target populations. This phage-driven enhancement of bacterial
387 competition introduces a novel layer of complexity to microbial interactions, emphasizing the dual

388 evolutionary pressures imposed by both phage predation and bacterial antagonism. Our findings
389 underscore the critical role phages play in influencing bacterial competition and shaping microbial
390 community structure. The interplay between bacterial defense mechanisms and phage-mediated
391 pressures indicates that, beyond their traditional role as predators, phages may act as indirect
392 facilitators of interbacterial interactions. This model establishes a framework for future studies to
393 investigate these dynamics across diverse microbial ecosystems and environmental contexts,
394 which is essential for a comprehensive understanding of microbial ecology.

395 Further research should focus on how these interactions influence the long-term stability
396 and composition of bacterial populations in natural settings. In addition, the therapeutic potential
397 of phage-derived enzymes, such as TSP, should be explored in greater detail, particularly given the
398 growing global threat of antibiotic resistance. Phage-derived enzymes could offer a novel approach
399 to antimicrobial therapy by targeting bacterial defenses and enhancing the efficacy of conventional
400 treatment strategies[83].

401

402 # METHODS

403 **Bacteria, bacteriophages, and culture conditions**

404 The bacterial and phage strains used in this study are listed in Supplementary Table 1. The
405 following *Escherichia coli* strains were used: DH5α and PIR1 for cloning and plasmid
406 maintenance; S17-1 λ pir for conjugal transfer of the pRE118 plasmid into *S. enterica*, *E. coli*, and
407 *C. rodentium*; and BL21 (DE3) for overproduction and purification of TSP protein samples.
408 *Salmonella enterica* serovar Typhimurium ATCC-14028, *Enterobacter cloacae* ATCC-13047, and
409 enterohemorrhagic *Escherichia coli* EDL933 were used for bacterial co-culture and competition
410 assays. Bacterial strains were routinely grown in Luria Bertani (LB) medium or Brain Heart

411 Infusion (BHI) medium with appropriate antibiotics at 37 °C and shaking at 200 rpm. Antibiotics
412 were used at the following concentrations: 50 μg/mL for kanamycin, 25 μg/mL for
413 chloramphenicol, 50 μg/mL for streptomycin, and 50 μg/mL for nalidixic acid.
414
415 **Plasmid construction**
416 All plasmids and primers used in our study are listed in Supplementary Table 1. In-frame
417 chromosomal deletions were created using pRE118 for *S. enterica*, *E. coli*, and *C. rodentium*. To
418 generate chromosomal mutation constructs, 800 bp regions flanking the mutation site were PCR
419 amplified, sewed together, and inserted into the vector via Gibson assembly at *XbaI* and *SacI*
420 restriction sites[84]. For P22 TSP purification constructs, the amino acid residues spanning 109-666
421 were PCR amplified and cloned into pETDuet-1 with N-terminal His6-tagged via Gibson assembly
422 at *BamHI* and *NotI* restriction sites. TSP catalytic mutant D392N was generated using site-directed
423 mutagenesis[85].
424
425 **Generation of mutant strains of *S. enterica*, *E. coli*, and *C. rodentium***
426 To generate deletions in *S. enterica*, *E. coli*, and *C. rodentium*, mutation constructs cloned
427 into pRE118 were transformed into conjugative *E. coli* S-17 λ pir[86]. Conjugative donor cells
428 carrying the deletion construct and recipient cells were grown overnight on LB plates containing
429 the appropriate antibiotics. The donor and recipient cells were then mixed at a 10:1 ratio, spotted
430 onto LB agar plates, and incubated at 37 °C for 6 hours to allow transfer of the deletion plasmid
431 via conjugation. The cell mixtures were scraped into LB medium and plated onto LB agar
432 supplemented with kanamycin and chloramphenicol (for *S. enterica* and *E. coli*) or kanamycin and
433 nalidixic acid (for *C. rodentium*) to select for cells containing the chromosomally inserted deletion

434 construct. The merodiploid strains were grown overnight in non-selective LB medium at 37 °C,
435 followed by counter-selection on nutrient agar supplemented with 10% (*w/v*) sucrose at room
436 temperature. Kanamycin-sensitive colonies were picked, and the deletions were confirmed by
437 colony PCR and Sanger sequencing. The chloramphenicol-resistant *S. enterica* and *E. coli* strains
438 were generated using pGRG37 methods[87].
439
440 **Phage propagation**
441 *S. enterica* ATCC-14028 was used as the host for phage propagation to obtain a high-titer
442 phage lysate (>10^8 PFU). An overnight culture was diluted in 50 mL of fresh LB broth to an OD_{600}
443 of 0.015 and incubated at 37 °C until the OD_{600} reached 0.2. Phage lysate was then added at a low
444 multiplicity of infection (MOI = 0.1), and the culture was incubated at 37 °C for 6 hours. After
445 incubation, the mixture was centrifuged at 6,000 x *g* for 10 minutes and filtered through a 0.2-µm
446 filter. The phage lysate was stored at 4 °C until use, and the phage titer was determined by spot
447 assays.
448
449 **Spot assay**
450 To calculate the phage titer, 100 µL of mid-log phase *S. enterica* (OD_{600} = 0.5 – 0.8) was mixed
451 with either 4 mL of prewarmed 0.7% (*w/v*) soft LB agar or 8 mL of 0.5% (*w/v*) soft BHI agar and
452 immediately poured onto 1.5% (*w/v*) regular LB agar plates. Then, 2 µL of 10-fold serially diluted
453 phage lysate was spotted onto the bacterial lawn. The plates were allowed to dry at room
454 temperature and subsequently incubated at 37 °C overnight. The number of visible single plaques
455 in each spot was counted to calculate the phage titer.
456

457 **Transposon mutant library construction**

458 The *S. enterica* transposon mutant library was constructed as described previously, with
459 slight modifications[88]. In brief, *S. enterica* cultures were harvested at mid-log phase (OD_{600} = 0.5)
460 and gently washed with sterilized 10% (*w/v*) glycerol. The EZ-Tn5<KAN-2> Tnp transposome
461 complex (Epicentre BioTechnologies) was added to the electrocompetent cells, which were
462 incubated on ice for 10 minutes. The mixture was then transferred to an ice-cold 1-mm
463 electroporation cuvette and electroporated at 2,450 V. Pre-warmed SOC medium was added, and
464 the cells were allowed to recover at 37 °C for 90 minutes. Tn5 mutants were selected on LB agar
465 plates containing kanamycin, pooled, and stored in LB medium with 50% (*w/v*) glycerol at -80 °C.
466 Approximately 12,000 Tn5::KanR insertion mutants were collected.

467

468 **Isolation of phage-resistant variants**

469 The *S. enterica* transposon library was inoculated into fresh LB broth containing
470 kanamycin and incubated at 37 °C until the culture reached the early log phase (OD_{600} = 0.2).
471 Phage lysate containing 10^8 PFU was then added to the culture, which was incubated at 37 °C for
472 1 hour. The OD_{600} was monitored hourly until the culture reached mid-log phase (OD_{600} = 0.5).
473 Bacterial samples from the infected culture were plated on LB agar containing kanamycin and
474 incubated at 37 °C overnight. Colonies of *S. enterica* that grew on the plates were picked and tested
475 for phage resistance by spot assay. To confirm that the phage-resistant variants were not lysogens,
476 the putative phage-resistant cells were treated with mitomycin C and plated on an *S. enterica* lawn
477 for further analysis.

478

479 **Identification of bacteriophage-resistant mutations**

480 The workflow for identifying phage-resistant mutations is depicted in Supplementary
481 Figure 2a. Phage-resistant strains were grown in LB broth at 37 °C overnight, followed by genomic
482 DNA (gDNA) extraction using a DNeasy Blood & Tissue Kit (Qiagen). Primer extension with
483 single primer (EzTn_s) was performed to amplify a fragment of the Tn5-gDNA junction. The
484 extension cycle included a manual hot start, with initial denaturation at 95 °C for 2 minutes,
485 followed by the addition of polymerase. The linear extension products were purified using
486 SPRIselect Bead-Based Reagent (Beckman Coulter). A deoxycytidine homopolymer tail (C-tail)
487 was added to the 3' end of the linear extension products using terminal deoxynucleotidyl
488 transferase (TdT; New England Biolabs). The reaction was carried out at 37 °C for 1 hour, followed
489 by enzyme inactivation at 75 °C for 20 minutes. The C-tailed products were then purified again
490 using SPRIselect Bead-Based Reagent. The purified C-tailed products were enriched by PCR using
491 Tn5_F and Tn5_R primers. Finally, the PCR products were heated at 65 °C for 15 minutes and
492 analyzed on 1.5% agarose gels. DNA fragments ranging from 300 to 500 bp were gel extracted for
493 Sanger sequencing and BLAST analysis.
494
495 **Monoculture bacterial growth in LB broth**
496 Bacteria were cultured overnight and subsequently diluted to an OD_{600} of 0.1 in LB broth.
497 A total of 100 μL of the diluted cells was transferred to 96-well, clear-bottom microplates, and the
498 growth rate was measured every 10 minutes for 12 hours using an Infinite F200 series plate reader
499 (Tecan). To prevent cell aggregation, 10 seconds of shaking was applied prior to each measurement.
500 Blank media and the wild-type strain were included on each plate, and at least three biological
501 replicates were measured for each sample.
502

503 **Monoculture bacterial growth on solid agar**

504 Overnight cultures grown in LB medium were pelleted, washed, and adjusted to an OD_{600}
505 = 20. Cell mixture (5 μL) was spotted onto nitrocellulose filters placed on LB agar plates and
506 incubated at 37 °C for 12 hours. Cells were then scraped from the nitrocellulose and resuspended
507 in 200 μL of LB broth. Initial and post-co-culture cell counts were determined by performing 10-
508 fold serial dilutions and plating the dilutions on LB agar plates containing the appropriate antibiotic.

509

510 **LPS analysis**

511 LPS was analyzed as previously described, with some modifications[89]. In brief, overnight
512 bacterial culture (10 OD_{600}) was pelleted and resuspended in 150 μL of Dissociation Buffer A (0.5
513 M Tris-HCl pH 6.8, 10% (*w/v*) glycerol, 10% (*w/v*) SDS, 5% (*v/v*) β-mercaptoethanol), followed
514 by boiling for 10 minutes. After cooling to room temperature, the samples were centrifuged at
515 18,000 x *g* for 15 minutes. The supernatant (100 μL) was diluted into 900 μL of Dissociation
516 Buffer B (0.5 M Tris-HCl pH 6.8, 10% (*w/v*) glycerol, 0.05% (w/v) bromophenol blue)
517 supplemented with 1 μL of 20 mg/mL proteinase K, and incubated at 37 °C for 1 hour. The samples
518 were separated on 12% or 20% (*w/v*) SDS-PAGE and stained using a Pro-Q Emerald 300
519 Lipopolysaccharide Gel Stain Kit (Invitrogen) for imaging.

520

521 **Transmission Electron Microscopy (TEM) analysis**

522 For TEM analysis, 4 μL droplets of phage lysate (~10^{10} PFU/mL) were placed on copper
523 grids (300 mesh) coated with a carbon-coated formvar film (Ted Pella Inc., Redding, CA). The
524 phage lysate was allowed to settle for 1 minute at room temperature and then dried using 3M filter
525 paper. Negative staining was performed with 1% (*w/v*) uranyl acetate for 30 seconds, after which

526 the excess stain was removed with 3M filter paper. The sample was gently washed three times with
527 sterilized distilled deionized water, and the grid was air-dried overnight at room temperature.
528 Phage morphology was visualized using a Talos 120 C transmission electron microscope (Thermo,
529 Waltham, US).
530

531 **Bacterial co-culture experiments**

532 Overnight cultures grown in LB medium were pelleted, washed, and adjusted to an OD_{600}
533 of 5 for liquid co-culture assays or to an OD_{600} of 20 for assays on solid agar. Cells were mixed at
534 a 1:1 ratio in LB broth and incubated at 37 °C for 1 hour. For solid agar experiments, 5 μL of the
535 cell mixture was spotted onto nitrocellulose filters placed on LB agar plates and incubated at 37
536 °C for 3 hours. Cells were then scraped from the nitrocellulose and resuspended in 200 μL of LB
537 broth. Initial and post-co-culture cell counts were determined by performing 10-fold serial
538 dilutions and plating the dilutions on LB agar plates containing the appropriate antibiotics. Relative
539 survival of the bacteria was calculated as the ratio of post-co-culture colony forming units (CFUs)
540 to the average CFUs of wild-type *S. enterica*.
541

542 **Macroscopic cell aggregation assay**

543 Macroscopic cell aggregation assays were performed as described previously, with slight
544 modifications[90]. Bacterial cultures were grown overnight at 37 °C in LB broth containing
545 kanamycin. After incubation, the cultures were vortexed and transferred to a 2-mm cuvette. The
546 bacterial cultures were then allowed to settle at room temperature for 22 hours to observe cell
547 aggregation.
548

549 **Bacterial competition assays**

550 Competition assays were performed as described previously, with slight modifications[91].
551 The bacterial strains used in the assays were cultured overnight at 37 °C, harvested by
552 centrifugation, washed, and resuspended in LB medium. *E. cloacae* was used as the donor strain,
553 whereas *S. enterica*, *E. coli*, and *C. rodentium* served as the recipient strains. Donor and recipient
554 cells were mixed at a 10:1 ratio, and a 5 μL aliquot of the mixture was spotted onto nitrocellulose
555 filters placed on pre-warmed LB agar plates. The plates were incubated at 37 °C for 1 hour. Cells
556 were then scraped from the nitrocellulose and resuspended in 200 μL of LB broth. Initial and post-
557 competition CFU counts were determined by performing 10-fold serial dilutions and plating on
558 LB agar plates containing the appropriate antibiotics. The bacterial relative protective index was
559 calculated as the ratio of the output recipient-to-donor ratio divided by the input recipient-to-donor
560 ratio, followed by normalization to the protective index of wild-type *S. enterica*.

561 To assess if phage-derived external modifiers of LPS could influence bacterial
562 susceptibility to T6SS-mediated attacks, wild-type *S. enterica* cells were treated with purified TSP
563 (10 nM), live phages (10^5 PFU/mL), or UV-inactivated phages (10^5 PFU/mL) for 10 minutes at 37
564 °C. Treated cells were then mixed with *E. cloacae* at a 10:1 donor-to-recipient ratio, and the
565 mixture was spotted onto nitrocellulose filters placed on pre-warmed LB agar plates. After
566 incubation at 37 °C for 1 hour, cells were collected by scraping them from the filters and
567 resuspending them in 200 μL of LB broth. Initial and post-co-culture CFU counts were determined
568 through serial dilutions and plating on LB agar with selective antibiotics. The bacterial relative
569 protective index was calculated as the ratio of the output recipient-to-donor ratio divided by the
570 input recipient-to-donor ratio and normalized to the protective index of wild-type *S. enterica*.

571

572 **P22 TSP purification**

573 Purification of recombinant P22 TSP (wild-type and D392N mutant) was performed as
574 described previously[92]. In brief, the N-terminal His^6-tagged TSP was expressed in *E. coli* BL21
575 (DE3). An overnight culture was diluted 100-fold into 1 L of LB medium containing carbenicillin
576 and incubated at 37 °C until the culture reached mid-log phase (OD_{600} = 0.6 - 0.8). TSP expression
577 was induced by adding 1 mM IPTG and incubating at 37 °C for 4 hours. Cells were harvested by
578 centrifugation at 4 °C and resuspended in 20 mL of resuspension buffer (20 mM Tris-HCl pH 7.5,
579 300 mM NaCl, 5 mM imidazole pH 7.0, 1 mM DTT, and a protease inhibitor cocktail). The
580 resuspended cells were disrupted by sonication, and cell debris was removed by centrifugation at
581 40,000 × *g* for 30 minutes at 4 °C. The soluble His^6-TSP was purified from the supernatant using
582 gravity flow through a 2 mL Ni-NTA agarose column. Bound proteins were eluted using a linear
583 imidazole gradient (25 to 300 mM). Purified proteins were analyzed by 12.5% (*w/v*) SDS-PAGE
584 followed by Coomassie Brilliant Blue staining.

585

586 **Bacteriophage inactivation by UV treatment**

587 The purified phage stock was diluted to ~10^9 PFU/mL, and 1 mL aliquots were placed in
588 Petri dishes covered with parafilm. The dishes were exposed to 254 nm UV light using a
589 Stratalinker UV Crosslinker 1800 (Stratagene, La Jolla, CA) for the indicated time intervals. Phage
590 infection efficiency following UV treatment was assessed by spot assay (Figure 5e, Supplementary
591 Figures 5c, d).

592

593 **Membrane permeability assays**

594 Outer membrane permeability was assessed using NPN uptake and VAN sensitivity assays,
595 as described previously[71, 93]. For the NPN uptake assay, mid-log phase cultures (OD_{600} = 0.5) were
596 pelleted and gently washed with 5 mM HEPES buffer (pH 7.2). An equal volume of HEPES buffer
597 containing 20 μM NPN was added to the samples and mixed thoroughly. As a control, 1 mM EDTA
598 was added to wild-type cells. Fluorescence was measured using an optical-bottom black plate in a
599 SpectraMax iD5 microplate reader (Molecular Devices) with excitation at 350 nm and emission at
600 420 nm, recorded at 30-second intervals for 10 minutes. Data collected over 10 minutes were
601 averaged, and NPN uptake activity was normalized by subtracting the background fluorescence in
602 the absence of NPN. For the VAN sensitivity assay, overnight cultures were diluted to an OD_{600} of
603 0.05 in 25 mL of LB broth, followed by the addition of 150 μg/mL vancomycin. As a control, 1
604 mM EDTA was added to wild-type cells. After 2 hours of incubation at 37 °C, CFUs were
605 determined by performing 10-fold serial dilutions and plating on LB agar.
606
607 **Atomic force microscopy (AFM)**
608 Atomic force microscopy (AFM) sample preparation was performed as described
609 previously, with some modifications[94]. An overnight bacterial culture was diluted 100-fold and
610 incubated at 37 °C until it reached mid-log phase (OD_{600} = 0.6 – 0.8). Cells were harvested by
611 centrifugation at OD_{600} = 1, washed, and then resuspended in 10 mM HEPES buffer (pH 7.4)[95].
612 For immobilization, 200 μL of the bacterial suspension was applied to freshly cleaved mica and
613 incubated for 20 minutes at room temperature. Following immobilization, the sample was gently
614 rinsed with Milli-Q water to remove any non-adherent cells, then air-dried in a desiccator for 30
615 minutes prior to AFM measurements.

616 AFM measurements were carried out using a Multimode NanoScope V system (Bruker
617 AXS) with PeakForce Tapping (PFT) and Force Volume (FV) mapping modes. A commercial tip
618 holder equipped with silicon (Si) cantilevers (FMAuD, NanoSensor), a spring constant of 2.0 N/m,
619 and a resonance frequency of 70.0 kHz was employed. PFT mode was used for high-resolution
620 imaging with a peak force setpoint of 1 nN and modulation of 2 kHz in the Z-ramp. For mechanical
621 mapping and force spectroscopy, FV mode was employed to collect force-distance (F-Z) curves
622 across the sample surface. Force spectroscopy was conducted using 32 × 32 pixels in the XY scan
623 area with 512 points per force curve at a 3 Hz Z-ramp for data acquisition and analysis. The force-
624 distance curves were calibrated from the original force-displacement (F-D) data following standard
625 processing protocols[96]. AFM imaging was restricted to isolated bacterial cells to prevent
626 confounding effects from cell aggregation. The AFM instrument was housed in a humidity-
627 controlled environment (~35%) to reduce capillary forces between the AFM tip and the bacterial
628 surface. Raw AFM images were processed and analyzed using Nanoscope Analysis software
629 (Bruker AXS).

630 To analyze force-distance curves, the initial jump-in force (point 1) was defined as the
631 contact point on the LPS layer, corresponding to a tip-sample distance of 0 nm and a tip-sample
632 interaction force of 0 nN. Two distinct interaction profiles from each force curve were identified
633 by slope changes, in which the increase of the slope represented the contact of a stiffer substrate.
634 The length of the LPS layer was measured as the distance between point 1 and point 2 (Figure 6g).
635 Ten force curves were obtained from multiple cells at different locations to ensure representative
636 sampling.

637

638 **Quantification and statistical analysis**

639 Statistical significance in bacterial conjugation and survival assays was assessed by
640 unpaired two-tailed t-tests between relevant samples. Details of statistical significance are
641 provided in the figure legends.
642

643 ## ACKNOWLEDGMENTS

644 We thank Ting laboratory members for helpful discussions and critical reading of the
645 manuscript; Dr. Joseph Mougous, Dr. Shu-Jung Chang, and Dr. Sue Lin-Chao for sharing reagents;
646 Dr. Soo-Chen Cheng and Dr. Jun-Yi Leu for sharing equipment; Dr. Shu-Yun Tung, Dr. Hsin-Nan
647 Lin, Dr. Chen-Hsin Yu, Ms. Wen-Li Pon, and Ms. Shin-Yi Du for technical assistance; and Dr.
648 John O'Brien for manuscript editing. We acknowledge funding support from Academia Sinica
649 (AS-CDA-112-L05 to S.-Y.T.) and the National Science and Technology Council, Taiwan (111-
650 2311-B-001-006-MY2, 112-2311-B-001-020, and 113-2628-B-001-008-MY3 to S.-Y.T.).
651

652 ## COMPETING INTERESTS

653 The authors declare no competing interests.
654

655 ## FIGURE LEGENDS

656

657 **Figure 1. Isolation of phage-resistant *S. enterica* for pairwise co-culture experiments. (a)**
658 Schematic workflow for isolating phage-resistant strains from a transposon library (Tn-library)
659 pool containing approximately 12,000 mutants. Phages from different families of Caudovirales
660 were used for selection: Felix O1, P22, and Chi (**Supplementary Figure 1a**). Spot assays were
661 employed to validate the resistance of the isolated strains to phage infections (**Supplementary**

662 **Figure 1b**). Validated resistant variants were subsequently co-cultured with *E. coli* or *E. cloacae*
663 in liquid broth or on solid agar. The survival of *S. enterica* was quantified by counting CFUs on
664 selective media. **(b, c)** Relative survival of the indicated *S. enterica* strains relative to wild-type *S.*
665 *enterica* grown in co-culture with *E. coli* or *E. cloacae* in LB broth **(b)** or solid agar **(c)**. Relative
666 survival was determined by comparing CFU ratios of phage-resistant variants and the wild-type
667 control. Data in **(b)** and **(c)** are represented as means ± SD (n=3). Asterisks indicate statistically
668 significant differences between the survival of a mutant strain and the wild-type control ($p < 0.05$).
669
670 **Figure 2. Phage-resistant strains exhibited LPS deficiency and increased susceptibility to**
671 **T6SS-mediated antagonism by *E. cloacae*. (a, b)** 12% LPS PAGE profiles showing the levels of
672 LPS produced by the indicated *S. enterica* strains: **(a)** LPS from the Felix O1-resistant strains; **(b)**
673 LPS from the P22-resistant strains. A schematic representation of LPS is shown on the left. **(c-h)**
674 Protectiveness of the indicated *S. enterica* phage-resistant strains relative to the wild-type strain
675 after competition with *E. cloacae* wild-type **(c, d)**, Δ*tssM* **(e, f)**, and Δ*cdiA* **(g, h)**. Data in **(c-h)** are
676 presented as means ± SD (n=6). Asterisks indicate statistically significant differences between the
677 relative protective index of a mutant strain and the wild-type control ($p < 0.05$).
678
679 **Figure 3. LPS protects bacteria from T6SS-mediated assaults. (a**) Schematic representation of
680 the LPS structure in *S. enterica*. Glycosyltransferases involved in LPS biosynthesis are indicated.
681 **(b, d, g)** Protectiveness of the indicated *S. enterica* mutant strains relative to the wild-type strain
682 after competition with wild-type *E. cloacae*. **(c, e, f)** LPS PAGE profiles: **(c)** 20% gel; **(e, f)** 12%
683 gel, showing LPS levels produced by the indicated *S. enterica* mutant strains. **(h)** Protectiveness
684 of the indicated bacterial species (Δ*waaO* mutant) relative to the wild-type strain after competition

685 with wild-type *E. cloacae*. **(i)** 12% LPS PAGE profiles showing LPS levels produced by the
686 indicated *S. enterica*, *E. coli*, and *C. rodentium* strains. Data in **(b, d, g, h)** are presented as means
687 ± SD (n=6). Asterisks indicate statistically significant differences between the relative protective
688 index of a mutant strain and the wild-type control ($p < 0.05$).
689
690 **Figure 4. Purified TSP increases the susceptibility of *S. enterica* to T6SS-mediated**
691 **intoxication. (a)** Schematic illustration of the phage P22. **(b)** Crystal structure of the P22 TSP
692 (PBD: 1TYX)[97] with the O-antigen substrate bound in the catalytic pocket. The D392 residue is
693 highlighted in pink. **(c)** Schematic representation of O-antigen digestion by phage P22 containing
694 enzymatically active TSP. **(d)** 12% LPS PAGE profiles showing LPS levels from wild-type *S.*
695 *enterica* treated with different concentrations of purified TSP (wild-type or D392N mutant) for 10
696 minutes at room temperature. LPS extracted from the Δ*waaL* strain is shown as a control. **(e)** 10-
697 fold serial dilution spot assay of P22 phage on wild-type *S. enterica* treated with 10 nM purified
698 TSP. The image is representative of triplicate experiments. **(f, g)** Protectiveness of the wild-type *S.*
699 *enterica* strain treated with purified TSP (wild-type or D392N mutant) relative to the mock-treated
700 *S. enterica* after competition with *E. cloacae* wild-type **(f)** or Δ*tssM* **(g)**. Data in **(f, g)** are presented
701 as means ± SD (n=6). Asterisks indicate statistically significant differences between the relative
702 protective index of TSP-treated *S. enterica* and the mock-treated control ($p < 0.05$).
703
704 **Figure 5. Phage P22 sensitizes *S. enterica* to T6SS-mediated attacks in mixed populations. (a)**
705 Schematic representation of phages with or without LPS-targeting endoglycosidase during
706 infection of *S. enterica*. *E. cloacae* carrying a functional T6SS is depicted at the top. **(b, c)**
707 Protectiveness of the wild-type *S. enterica* strain treated with different phages (Felix O1, P22, or

708 Chi) relative to the mock-treated *S. enterica* after competition with *E. cloacae* wild-type **(b)** or
709 Δ*tssM* **(c)**. **(d)** Schematic of P22 with UV_{254nm} treatment. **(e)** 10-fold serial dilution spot assay of
710 UV-inactivated P22 phage on wild-type *S. enterica*. The image is representative of triplicate
711 experiments. **(f, g)** Protectiveness of the wild-type *S. enterica* strain treated with UV-inactivated
712 phage particles (Felix O1, P22, or Chi) relative to the mock-treated *S. enterica* after competition
713 with *E. cloacae* wild-type **(f)** or Δ*tssM* **(g)**. Data in **(b, c, f, g)** are presented as means ± SD (n=6).
714 Asterisks indicate statistically significant differences between the relative protective index of
715 phage-treated or UV-inactivated phage-treated *S. enterica* and the mock-treated control ($p < 0.05$).
716
717 **Figure 6. Evidence that the O-antigen of LPS serves as a physical barrier. (a, b)** Measurements
718 of outer membrane permeability of *S. enterica* wild-type, Δ*wzzB*, and Δ*waaL*. 1 mM EDTA was
719 added to the wild-type as the control. **(a)** NPN uptake assay; **(b)** VAN sensitivity assay. **(c)**
720 Schematic representation of the atomic force microscopy (AFM) setup. *S. enterica* cells were
721 immobilized on freshly prepared mica substrates. A laser beam reflected on the back of the
722 cantilever is used to measure the force interactions between the probe and sample. The feedback
723 control system between the photodetector and the X-Y-Z scanner enables precise detection of the
724 surface morphology of the cells. (Zoom-in) A detailed view of the AFM measurement on the
725 bacterial surface. **(d-f)** AFM height images of *S. enterica* wild-type **(d)**, Δ*wzzB* **(e)**, and Δ*waaL* **(f)**
726 were obtained using PeakForce Tapping (PFT) mode. The image scan size is 1 μm x 1 μm. **(g)**
727 Schematic of the AFM force-distance curve obtained from *S. enterica* samples using Force Volume
728 (FV) mapping mode. The point at which the tip contacts the sample is defined as zero (point 1),
729 while slope changes indicate a transition to a stiffer substrate (point 2). **(h-j)** Force-distance curves
730 from *S. enterica* wild-type **(h)**, Δ*wzzB* **(i)**, and Δ*waaL* **(j)**. Ten curves were captured from each

731 sample at randomly selected locations, with the longest and shortest LPS lengths highlighted. Red
732 arrows mark points 1 and 2. **(k)** LPS length of *S. enterica* wild-type, Δ*wzzB*, and Δ*waaL* was
733 determined from force-distance curves by measuring the distance between point 1 and point 2.
734
735 **Figure 7. Working model of how phages modulate interbacterial competition within**
736 **microbial communities.** Bacterial interactions are shaped either in the absence (left) or presence
737 (right) of phages. **(a)** Bacteria inhabit polymorphic environments. **(b)** In the presence of P22 phage,
738 bacterial surfaces can be modified via two distinct mechanisms. **(c)** LPS-modified strains are
739 selected due to their resistance to phage adsorption, leading to their dominance within *S. enterica*
740 populations. **(d)** TSP from the P22 phage specifically cleaves the bacterial O-antigen of LPS,
741 resulting in a shortened structure. **(e)** LPS deficiency increases the susceptibility of *S. enterica* to
742 contact-dependent killing by close proximity bacterial competitors. **(f)** Phage-mediated surface
743 modifications influence the outcome of interbacterial competition, driving dynamic shifts in mixed
744 bacterial populations.
745
746 **Figure S1. Validation of phage resistance in isolated mutants and monocultural growth**
747 **experiment. (a)** TEM images of model phages used in the study: Felix O1 (left), P22 (middle),
748 and Chi (right). Scale bar = 0.1 μm. **(b)** 10-fold serial dilution spot assay of phages Felix O1 (left),
749 P22 (middle), and Chi (right) on the indicated phage-resistant *S. enterica* strains. The image is
750 representative of triplicate experiments. **(c)** Growth curves of the indicated phage-resistant *S.*
751 *enterica* strains in LB broth at 37 °C. Wild-type, Δ*waaL*, and Δ*waaG* strains are shown as controls.
752 **(d)** CFUs of the indicated phage-resistant *S. enterica* strains grown at 37 °C for 12 hours on LB
753 agar plates. Wild-type, Δ*waaL* (ΔL), and Δ*waaG* (ΔG) strains are shown as controls.

754

755 **Figure S2. Characterization of transposon insertion mutations in phage-resistant *S. enterica***
756 **isolates. (a)** Schematic workflow for identifying phage-resistant mutations. Detailed procedures
757 are provided in the Methods section. **(b)** Mutated genes in the P22-resistant and Felix O1-resistant
758 *S. enterica* isolates. Scale bar = 500 bp. **(c)** Mutated genes in the Chi-resistant *S. enterica* isolates.
759 Scale bar = 1000 bp. **(d)** 12% LPS PAGE profiles showing LPS levels from the indicated Chi-
760 resistant *S. enterica* strains. A schematic representation of LPS is shown on the left. **(e, f)**
761 Macroscopic aggregation analysis to assess LPS deficiency in the indicated Felix O1-resistant **(e)**
762 or P22-resistant **(f)** *S. enterica* strains. The images are representative of triplicate experiments.

763

764 **Figure S3. LPS-deficient *S. enterica* mutants shows no significant growth or competition**
765 **defects. (a-c)** Growth curves of the indicated *S. enterica* LPS mutants in LB broth at 37 °C. The
766 wild-type strain is shown as a control. **(d-f)** Protectiveness of the indicated *S. enterica* mutant
767 strains relative to the wild-type strain after competition with *E. cloacae* Δ*tssM*. **(g)** Protectiveness
768 of the indicated bacterial species (Δ*waaO* mutant) relative to the wild-type strain after competition
769 with *E. cloacae* Δ*tssM*. Data in **(d-g)** are presented as means ± SD (n=6).

770

771 **Figure S4. TSP-treated *S. enterica* shows no significant growth defect. (a)** Coomassie-stained
772 12.5% SDS-PAGE analysis of the purified TSP (left) and the D392N catalytic mutant (right). **(b)**
773 Growth curves of wild-type *S. enterica* incubated with 10 nM of purified TSP (wild-type or D392N
774 mutant) at 37 °C. Mock-treated wild-type *S. enterica* and the Δ*waaL* mutant are shown as controls.

775

776 **Figure S5. Supporting evidence that phage P22 sensitizes *S. enterica* to T6SS-mediated**
777 **attacks. (a)** 10-fold serial dilution spot assay of phages Felix O1 (left), P22 (middle), and Chi
778 (right) on wild-type *S. enterica* before and after the competition assay (Figure 5b). **(b)** 10-fold
779 serial dilution spot assay of phages Felix O1 (left), P22 (middle), and Chi (right) on wild-type *S.*
780 *enterica* and *E. cloacae.* **(c, d)** 10-fold serial dilution spot assay of UV-inactivated Felix O1 phage
781 **(c)** or Chi phage **(d)** on wild-type *S. enterica*. The images are representative of triplicate
782 experiments.
783
784 **Figure S6. The slope of AFM force-distance curves.** Two distinct slopes from each force-
785 distance curve were obtained for *S. enterica* wild-type, Δ*wzzB*, and Δ*waaL* strains. Ten curves were
786 divided into two segments by point 2, as shown in Figure 6g. The slope measured from the first
787 segment corresponds to the LPS layer (left), while the second segment represents the outer
788 membrane (right).
789
790 **Supplementary Table 1.** Strains, Recombinant DNA, and Oligonucleotides used in this study.
791

792 ## AUTHOR CONTRIBUTIONS

793 C.-E.T., F.-Q.W., C.-W.Y., I.-S.H., P.-Y.C., and S.-Y.T. designed the study. C.-E.T., F.-Q.W.,
794 C.-W.Y., L.-L.Y., and Y.-C.C. performed experiments. C.-E.T., F.-Q.W., C.-W.Y., I.-S.H., and S.-
795 Y.T. analyzed data. C.-E.T., F.-Q.W., C.-W.Y., P.-Y.C., I.-S.H., and S.-Y.T. wrote the manuscript.

796 ## REFERENCES

797 1. Brussow, H. & Hendrix, R.W. Phage genomics: small is beautiful. *Cell* **108**, 13-16 (2002).
798 2. Garcia-Bayona, L. & Comstock, L.E. Bacterial antagonism in host-associated microbial
799 communities. *Science* **361** (2018).

3. Cotter, P.D., Ross, R.P. & Hill, C. Bacteriocins - a viable alternative to antibiotics? *Nat Rev Microbiol* **11**, 95-105 (2013).
4. Klein, T.A., Ahmad, S. & Whitney, J.C. Contact-Dependent Interbacterial Antagonism Mediated by Protein Secretion Machines. *Trends Microbiol* **28**, 387-400 (2020).
5. Chassaing, B. & Cascales, E. Antibacterial Weapons: Targeted Destruction in the Microbiota. *Trends Microbiol* **26**, 329-338 (2018).
6. Hoque, M.M., Espinoza-Vergara, G. & McDougald, D. Protozoan predation as a driver of diversity and virulence in bacterial biofilms. *FEMS Microbiol Rev* **47** (2023).
7. Smith, W.P.J., Wucher, B.R., Nadell, C.D. & Foster, K.R. Bacterial defences: mechanisms, evolution and antimicrobial resistance. *Nat Rev Microbiol* **21**, 519-534 (2023).
8. Murtazalieva, K., Mu, A., Petrovskaya, A. & Finn, R.D. The growing repertoire of phage anti-defence systems. *Trends Microbiol* (2024).
9. Kulikov, E.E., Golomidova, A.K., Prokhorov, N.S., Ivanov, P.A. & Letarov, A.V. High-throughput LPS profiling as a tool for revealing of bacteriophage infection strategies. *Sci Rep* **9**, 2958 (2019).
10. Kaur, G., Agarwal, R. & Sharma, R.K. Bacteriophage Therapy for Critical and High-Priority Antibiotic-Resistant Bacteria and Phage Cocktail-Antibiotic Formulation Perspective. *Food Environ Virol* **13**, 433-446 (2021).
11. Doron, S. *et al.* Systematic discovery of antiphage defense systems in the microbial pangenome. *Science* **359** (2018).
12. Vassallo, C.N., Doering, C.R., Littlehale, M.L., Teodoro, G.I.C. & Laub, M.T. A functional selection reveals previously undetected anti-phage defence systems in the E. coli pangenome. *Nat Microbiol* **7**, 1568-1579 (2022).
13. Kennedy, N.W. & Comstock, L.E. Mechanisms of bacterial immunity, protection, and survival during interbacterial warfare. *Cell Host Microbe* **32**, 794-803 (2024).
14. Peterson, S.B., Bertolli, S.K. & Mougous, J.D. The Central Role of Interbacterial Antagonism in Bacterial Life. *Curr Biol* **30**, R1203-R1214 (2020).
15. Hersch, S.J. *et al.* Envelope stress responses defend against type six secretion system attacks independently of immunity proteins. *Nat Microbiol* **5**, 706-714 (2020).
16. Cornforth, D.M. & Foster, K.R. Competition sensing: the social side of bacterial stress responses. *Nat Rev Microbiol* **11**, 285-293 (2013).
17. LeRoux, M., Peterson, S.B. & Mougous, J.D. Bacterial danger sensing. *J Mol Biol* **427**, 3744-3753 (2015).
18. Mangalea, M.R. & Duerkop, B.A. Fitness Trade-Offs Resulting from Bacteriophage Resistance Potentiate Synergistic Antibacterial Strategies. *Infect Immun* **88** (2020).
19. Chan, B.K. *et al.* Phage selection restores antibiotic sensitivity in MDR Pseudomonas aeruginosa. *Sci Rep* **6**, 26717 (2016).
20. Levin, B.R. & Bull, J.J. Population and evolutionary dynamics of phage therapy. *Nat Rev Microbiol* **2**, 166-173 (2004).
21. Yu, T. *et al.* Sub-MIC antibiotics increased the fitness cost of CRISPR-Cas in Acinetobacter baumannii. *Front Microbiol* **15**, 1381749 (2024).
22. Vale, P.F. *et al.* Costs of CRISPR-Cas-mediated resistance in Streptococcus thermophilus. *Proc Biol Sci* **282**, 20151270 (2015).
23. Westra, E.R. *et al.* Parasite Exposure Drives Selective Evolution of Constitutive versus Inducible Defense. *Curr Biol* **25**, 1043-1049 (2015).

845 24. Meaden, S. *et al.* Correction: Phage gene expression and host responses lead to infection-
846 dependent costs of CRISPR immunity. *ISME J* **15**, 2491 (2021).
847 25. Zaayman, M. & Wheatley, R.M. Fitness costs of CRISPR-Cas systems in bacteria.
848 *Microbiology (Reading)* **168** (2022).
849 26. Chaudhry, W. *et al.* Mucoidy, a general mechanism for maintaining lytic phage in
850 populations of bacteria. *FEMS Microbiol Ecol* **96** (2020).
851 27. Wielgoss, S., Bergmiller, T., Bischofberger, A.M. & Hall, A.R. Adaptation to Parasites and
852 Costs of Parasite Resistance in Mutator and Nonmutator Bacteria. *Mol Biol Evol* **33**, 770-
853 782 (2016).
854 28. Scanlan, P.D. & Buckling, A. Co-evolution with lytic phage selects for the mucoid
855 phenotype of Pseudomonas fluorescens SBW25. *ISME J* **6**, 1148-1158 (2012).
856 29. MacGillivray, K.A. *et al.* Trade-offs constrain adaptive pathways to the type VI secretion
857 system survival. *iScience* **26**, 108332 (2023).
858 30. Gomez, P. & Buckling, A. Bacteria-phage antagonistic coevolution in soil. *Science* **332**,
859 106-109 (2011).
860 31. York, D., Welch, K., Goryshin, I.Y. & Reznikoff, W.S. Simple and efficient generation in
861 vitro of nested deletions and inversions: Tn5 intramolecular transposition. *Nucleic Acids*
862 *Res* **26**, 1927-1933 (1998).
863 32. Trotereau, J. *et al.* Construction and characterization of a saturated Tn-seq library of
864 Salmonella Typhimurium ATCC 14028. *Microbiol Resour Announc* **12**, e0036523 (2023).
865 33. Whichard, J.M. *et al.* Complete genomic sequence of bacteriophage felix o1. *Viruses* **2**,
866 710-730 (2010).
867 34. Vander Byl, C. & Kropinski, A.M. Sequence of the genome of Salmonella bacteriophage
868 P22. *J Bacteriol* **182**, 6472-6481 (2000).
869 35. Lee, J.H., Shin, H., Choi, Y. & Ryu, S. Complete genome sequence analysis of bacterial-
870 flagellum-targeting bacteriophage chi. *Arch Virol* **158**, 2179-2183 (2013).
871 36. Nguyen, Y. & Sperandio, V. Enterohemorrhagic E. coli (EHEC) pathogenesis. *Front Cell*
872 *Infect Microbiol* **2**, 90 (2012).
873 37. Davin-Regli, A. & Pages, J.M. Enterobacter aerogenes and Enterobacter cloacae; versatile
874 bacterial pathogens confronting antibiotic treatment. *Front Microbiol* **6**, 392 (2015).
875 38. Galan, J.E. Salmonella Typhimurium and inflammation: a pathogen-centric affair. *Nat Rev*
876 *Microbiol* **19**, 716-725 (2021).
877 39. Vis, M.A.M., Ito, K. & Hofmann, S. Impact of Culture Medium on Cellular Interactions in
878 in vitro Co-culture Systems. *Front Bioeng Biotechnol* **8**, 911 (2020).
879 40. Rostol, J.T. & Marraffini, L. (Ph)ighting Phages: How Bacteria Resist Their Parasites. *Cell*
880 *Host Microbe* **25**, 184-194 (2019).
881 41. Baxa, U. *et al.* Interactions of phage P22 tails with their cellular receptor, Salmonella O-
882 antigen polysaccharide. *Biophys J* **71**, 2040-2048 (1996).
883 42. Hudson, H.P., Lindberg, A.A. & Stocker, B.A. Lipopolysaccharide core defects in
884 Salmonella typhimurium mutants which are resistant to Felix O phage but retain smooth
885 character. *J Gen Microbiol* **109**, 97-112 (1978).
886 43. Nakao, R., Ramstedt, M., Wai, S.N. & Uhlin, B.E. Enhanced biofilm formation by
887 Escherichia coli LPS mutants defective in Hep biosynthesis. *PLoS One* **7**, e51241 (2012).
888 44. Ge, H. *et al.* The rfbN gene of Salmonella Typhimurium mediates phage adsorption by
889 modulating biosynthesis of lipopolysaccharide. *Microbiol Res* **250**, 126803 (2021).

890 45. Beck, C.M. *et al.* CdiA from Enterobacter cloacae delivers a toxic ribosomal RNase into
891 target bacteria. *Structure* **22**, 707-718 (2014).
892 46. Whitney, J.C. *et al.* Genetically distinct pathways guide effector export through the type
893 VI secretion system. *Mol Microbiol* **92**, 529-542 (2014).
894 47. Hood, R.D. *et al.* A type VI secretion system of Pseudomonas aeruginosa targets a toxin to
895 bacteria. *Cell Host Microbe* **7**, 25-37 (2010).
896 48. Aoki, S.K. *et al.* Contact-dependent inhibition of growth in Escherichia coli. *Science* **309**,
897 1245-1248 (2005).
898 49. Hersch, S.J., Manera, K. & Dong, T.G. Defending against the Type Six Secretion System:
899 beyond Immunity Genes. *Cell Rep* **33**, 108259 (2020).
900 50. Toska, J., Ho, B.T. & Mekalanos, J.J. Exopolysaccharide protects Vibrio cholerae from
901 exogenous attacks by the type 6 secretion system. *Proc Natl Acad Sci U S A* **115**, 7997-
902 8002 (2018).
903 51. Flaugnatti, N. *et al.* Human commensal gut Proteobacteria withstand type VI secretion
904 attacks through immunity protein-independent mechanisms. *Nat Commun* **12**, 5751 (2021).
905 52. West, N.P. *et al.* Optimization of virulence functions through glucosylation of Shigella LPS.
906 *Science* **307**, 1313-1317 (2005).
907 53. Papo, N. & Shai, Y. A molecular mechanism for lipopolysaccharide protection of Gram-
908 negative bacteria from antimicrobial peptides. *J Biol Chem* **280**, 10378-10387 (2005).
909 54. Bertani, B. & Ruiz, N. Function and Biogenesis of Lipopolysaccharides. *EcoSal Plus* **8**
910 (2018).
911 55. Kaniuk, N.A., Vinogradov, E. & Whitfield, C. Investigation of the structural requirements
912 in the lipopolysaccharide core acceptor for ligation of O antigens in the genus Salmonella:
913 WaaL "ligase" is not the sole determinant of acceptor specificity. *J Biol Chem* **279**, 36470-
914 36480 (2004).
915 56. Di Lorenzo, F. *et al.* A Journey from Structure to Function of Bacterial Lipopolysaccharides.
916 *Chem Rev* **122**, 15767-15821 (2022).
917 57. Bastin, D.A., Stevenson, G., Brown, P.K., Haase, A. & Reeves, P.R. Repeat unit
918 polysaccharides of bacteria: a model for polymerization resembling that of ribosomes and
919 fatty acid synthetase, with a novel mechanism for determining chain length. *Mol Microbiol*
920 **7**, 725-734 (1993).
921 58. Murray, G.L., Attridge, S.R. & Morona, R. Regulation of Salmonella typhimurium
922 lipopolysaccharide O antigen chain length is required for virulence; identification of FepE
923 as a second Wzz. *Mol Microbiol* **47**, 1395-1406 (2003).
924 59. Zhang, G., Meredith, T.C. & Kahne, D. On the essentiality of lipopolysaccharide to Gram-
925 negative bacteria. *Curr Opin Microbiol* **16**, 779-785 (2013).
926 60. Simpson, B.W. & Trent, M.S. Pushing the envelope: LPS modifications and their
927 consequences. *Nat Rev Microbiol* **17**, 403-416 (2019).
928 61. Steinbacher, S. *et al.* Phage P22 tailspike protein: crystal structure of the head-binding
929 domain at 2.3 A, fully refined structure of the endorhamnosidase at 1.56 A resolution, and
930 the molecular basis of O-antigen recognition and cleavage. *J Mol Biol* **267**, 865-880 (1997).
931 62. Eriksson, U., Svenson, S.B., Lonngren, J. & Lindberg, A.A. Salmonella phage glycanases:
932 substrate specificity of the phage P22 endo-rhamnosidase. *J Gen Virol* **43**, 503-511 (1979).
933 63. Steinbacher, S. *et al.* Crystal structure of P22 tailspike protein: interdigitated subunits in a
934 thermostable trimer. *Science* **265**, 383-386 (1994).

935 64. Waseh, S. *et al.* Orally administered P22 phage tailspike protein reduces salmonella
936 colonization in chickens: prospects of a novel therapy against bacterial infections. *PLoS*
937 *One* **5**, e13904 (2010).
938 65. Tang, J. *et al.* Peering down the barrel of a bacteriophage portal: the genome packaging
939 and release valve in p22. *Structure* **19**, 496-502 (2011).
940 66. Sonani, R.R., Esteves, N.C., Scharf, B.E. & Egelman, E.H. Cryo-EM structure of
941 flagellotropic bacteriophage Chi. *Structure* **32**, 856-865 e853 (2024).
942 67. Snyder, D.S. & McIntosh, T.J. The lipopolysaccharide barrier: correlation of antibiotic
943 susceptibility with antibiotic permeability and fluorescent probe binding kinetics.
944 *Biochemistry* **39**, 11777-11787 (2000).
945 68. Delcour, A.H. Outer membrane permeability and antibiotic resistance. *Biochim Biophys*
946 *Acta* **1794**, 808-816 (2009).
947 69. Zgurskaya, H.I., Lopez, C.A. & Gnanakaran, S. Permeability Barrier of Gram-Negative
948 Cell Envelopes and Approaches To Bypass It. *ACS Infect Dis* **1**, 512-522 (2015).
949 70. Vaara, M. Agents that increase the permeability of the outer membrane. *Microbiol Rev* **56**,
950 395-411 (1992).
951 71. Helander, I.M. & Mattila-Sandholm, T. Fluorometric assessment of gram-negative
952 bacterial permeabilization. *J Appl Microbiol* **88**, 213-219 (2000).
953 72. Bolla, J.M. *et al.* Strategies for bypassing the membrane barrier in multidrug resistant
954 Gram-negative bacteria. *FEBS Lett* **585**, 1682-1690 (2011).
955 73. Wang, Z., Wang, J., Ren, G., Li, Y. & Wang, X. Influence of Core Oligosaccharide of
956 Lipopolysaccharide to Outer Membrane Behavior of Escherichia coli. *Mar Drugs* **13**,
957 3325-3339 (2015).
958 74. Allsopp, L.P. & Bernal, P. Killing in the name of: T6SS structure and effector diversity.
959 *Microbiology (Reading)* **169** (2023).
960 75. Dufrene, Y.F. Atomic force microscopy, a powerful tool in microbiology. *J Bacteriol* **184**,
961 5205-5213 (2002).
962 76. Strauss, J., Burnham, N.A. & Camesano, T.A. Atomic force microscopy study of the role
963 of LPS O-antigen on adhesion of E. coli. *J Mol Recognit* **22**, 347-355 (2009).
964 77. Kahli, H. *et al.* Impact of Growth Conditions on Pseudomonas fluorescens Morphology
965 Characterized by Atomic Force Microscopy. *Int J Mol Sci* **23** (2022).
966 78. Pagnout, C. *et al.* Pleiotropic effects of rfa-gene mutations on Escherichia coli envelope
967 properties. *Sci Rep* **9**, 9696 (2019).
968 79. Souza, D.P. *et al.* Bacterial killing via a type IV secretion system. *Nat Commun* **6**, 6453
969 (2015).
970 80. Bayer-Santos, E. *et al.* The opportunistic pathogen Stenotrophomonas maltophilia utilizes
971 a type IV secretion system for interbacterial killing. *PLoS Pathog* **15**, e1007651 (2019).
972 81. Sgro, G.G. *et al.* Bacteria-Killing Type IV Secretion Systems. *Front Microbiol* **10**, 1078
973 (2019).
974 82. Wang, H., Liu, Y., Bai, C. & Leung, S.S.Y. [Not Available]. *Acta Pharm Sin B* **14**, 155-169
975 (2024).
976 83. Knecht, L.E., Veljkovic, M. & Fieseler, L. Diversity and Function of Phage Encoded
977 Depolymerases. *Front Microbiol* **10**, 2949 (2019).
978 84. Gibson, D.G. *et al.* Enzymatic assembly of DNA molecules up to several hundred kilobases.
979 *Nat Methods* **6**, 343-345 (2009).

980 85. Kunkel, T.A. Rapid and efficient site-specific mutagenesis without phenotypic selection.
981 *Proc Natl Acad Sci U S A* **82**, 488-492 (1985).
982 86. Edwards, R.A., Keller, L.H. & Schifferli, D.M. Improved allelic exchange vectors and their
983 use to analyze 987P fimbria gene expression. *Gene* **207**, 149-157 (1998).
984 87. McKenzie, G.J. & Craig, N.L. Fast, easy and efficient: site-specific insertion of transgenes
985 into enterobacterial chromosomes using Tn7 without need for selection of the insertion
986 event. *BMC Microbiol* **6**, 39 (2006).
987 88. Mandal, R.K., Jiang, T. & Kwon, Y.M. Genetic Determinants in Salmonella enterica
988 Serotype Typhimurium Required for Overcoming In Vitro Stressors in the Mimicking Host
989 Environment. *Microbiol Spectr* **9**, e0015521 (2021).
990 89. Liu, Q. *et al.* Immunogenicity and Cross-Protective Efficacy Induced by Outer Membrane
991 Proteins from Salmonella Typhimurium Mutants with Truncated LPS in Mice. *Int J Mol*
992 *Sci* **17**, 416 (2016).
993 90. Chen, P.Y. *et al.* A whole-cell platform for discovering synthetic cell adhesion molecules
994 in bacteria. *Nat Commun* **15**, 6568 (2024).
995 91. Ting, S.Y. *et al.* Targeted Depletion of Bacteria from Mixed Populations by Programmable
996 Adhesion with Antagonistic Competitor Cells. *Cell Host Microbe* **28**, 313-321 e316 (2020).
997 92. Miller, S., Schuler, B. & Seckler, R. Phage P22 tailspike protein: removal of head-binding
998 domain unmasks effects of folding mutations on native-state thermal stability. *Protein Sci*
999 **7**, 2223-2232 (1998).
1000 93. Muheim, C. *et al.* Increasing the permeability of Escherichia coli using MAC13243. *Sci*
1001 *Rep* **7**, 17629 (2017).
1002 94. Oh, Y.J. Use of Atomic Force Microscopy to Characterize LPS Perturbations. *Methods Mol*
1003 *Biol* **2548**, 279-287 (2022).
1004 95. Singh, S. *et al.* LPS O Antigen Plays a Key Role in Klebsiella pneumoniae Capsule
1005 Retention. *Microbiol Spectr* **10**, e0151721 (2022).
1006 96. Gavara, N. A beginner's guide to atomic force microscopy probing for cell mechanics.
1007 *Microsc Res Tech* **80**, 75-84 (2017).
1008 97. Steinbacher, S. *et al.* Crystal structure of phage P22 tailspike protein complexed with
1009 Salmonella sp. O-antigen receptors. *Proc Natl Acad Sci U S A* **93**, 10584-10588 (1996).
1010

Figure 1

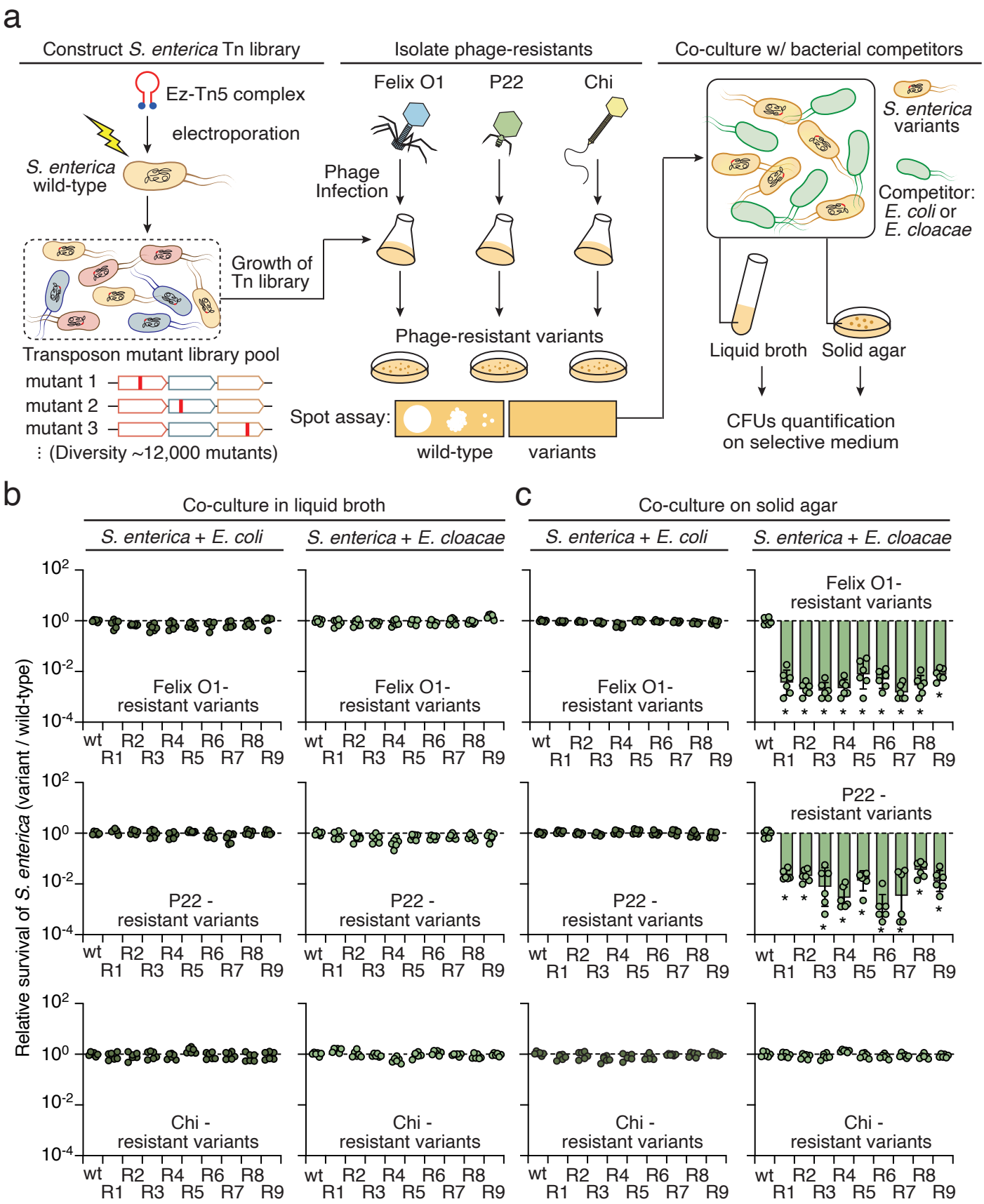
a
Construct S. enterica Tn library
Isolate phage-resistants
Co-culture w/ bacterial competitors
Ez-Tn5 complex
electroporation
S. enterica wild-type
Growth of Tn library
Transposon mutant library pool
mutant 1
mutant 2
mutant 3
⋮ (Diversity ~12,000 mutants)
Felix O1
P22
Chi
Phage Infection
Phage-resistant variants
Spot assay:
wild-type
variants
S. enterica variants
Competitor: E. coli or E. cloacae
Liquid broth
Solid agar
CFUs quantification on selective medium
b
Co-culture in liquid broth
S. enterica + E. coli
S. enterica + E. cloacae
c
Co-culture on solid agar
Relative survival of S. enterica (variant / wild-type)
Felix O1-resistant variants
P22 - resistant variants
Chi - resistant variants
wt R1 R2 R3 R4 R5 R6 R7 R8 R9

Figure 2

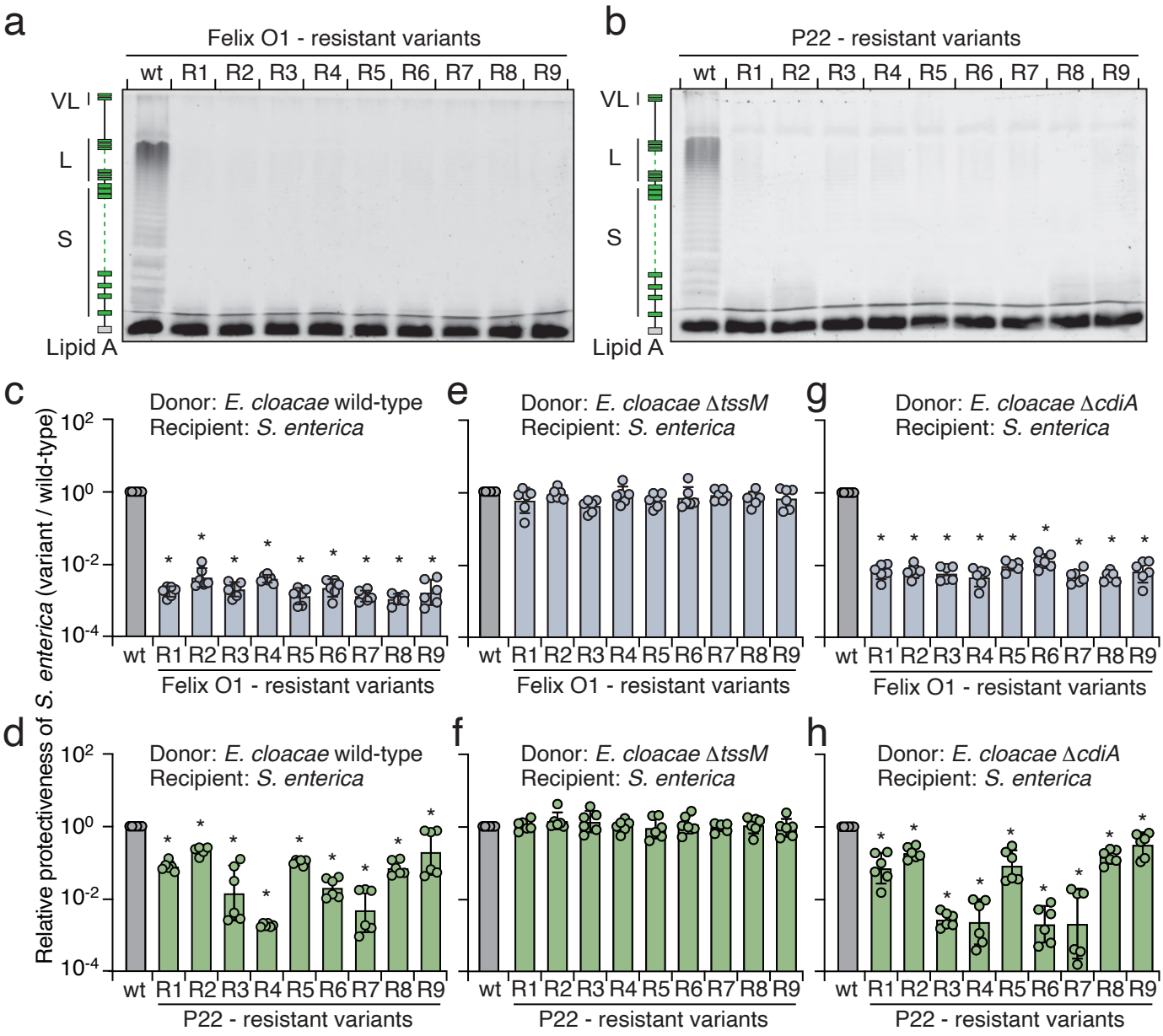
a
Felix O1 - resistant variants
wt R1 R2 R3 R4 R5 R6 R7 R8 R9
VL
L
S
Lipid A
b
P22 - resistant variants
wt R1 R2 R3 R4 R5 R6 R7 R8 R9
VL
L
S
Lipid A
c
Donor: E. cloacae wild-type
Recipient: S. enterica
e
Donor: E. cloacae ΔtssM
Recipient: S. enterica
g
Donor: E. cloacae ΔcdiA
Recipient: S. enterica
Felix O1 - resistant variants
d
Donor: E. cloacae wild-type
Recipient: S. enterica
f
Donor: E. cloacae ΔtssM
Recipient: S. enterica
h
Donor: E. cloacae ΔcdiA
Recipient: S. enterica
P22 - resistant variants
Relative protectiveness of S. enterica (variant / wild-type)
10^2
10^0
10^-2
10^-4
wt R1 R2 R3 R4 R5 R6 R7 R8 R9

Figure 3

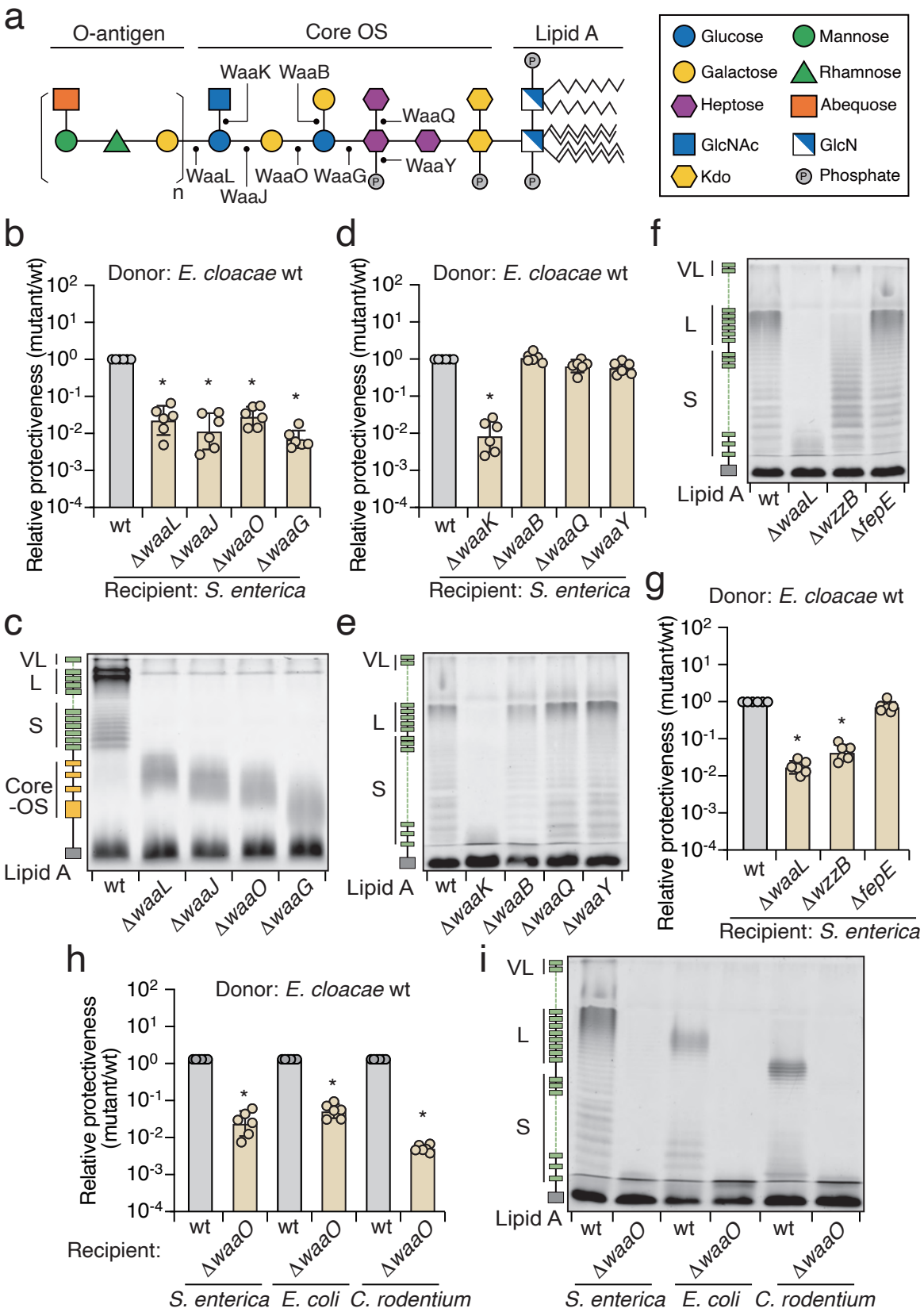
a
O-antigen
Core OS
Lipid A
WaaK
WaaB
WaaQ
WaaY
WaaL
WaaO
WaaG
WaaJ
n
Glucose
Mannose
Galactose
Rhamnose
Heptose
Abequose
GlcNAc
GlcN
Kdo
Phosphate
b
Donor: E. cloacae wt
Relative protectiveness (mutant/wt)
wt
ΔwaaL
ΔwaaJ
ΔwaaO
ΔwaaG
Recipient: S. enterica
c
VL
L
S
Core -OS
Lipid A
d
Donor: E. cloacae wt
ΔwaaK
ΔwaaB
ΔwaaQ
ΔwaaY
e
f
ΔwzzB
ΔfepE
g
h
Recipient:
S. enterica
E. coli
C. rodentium
i

Figure 4

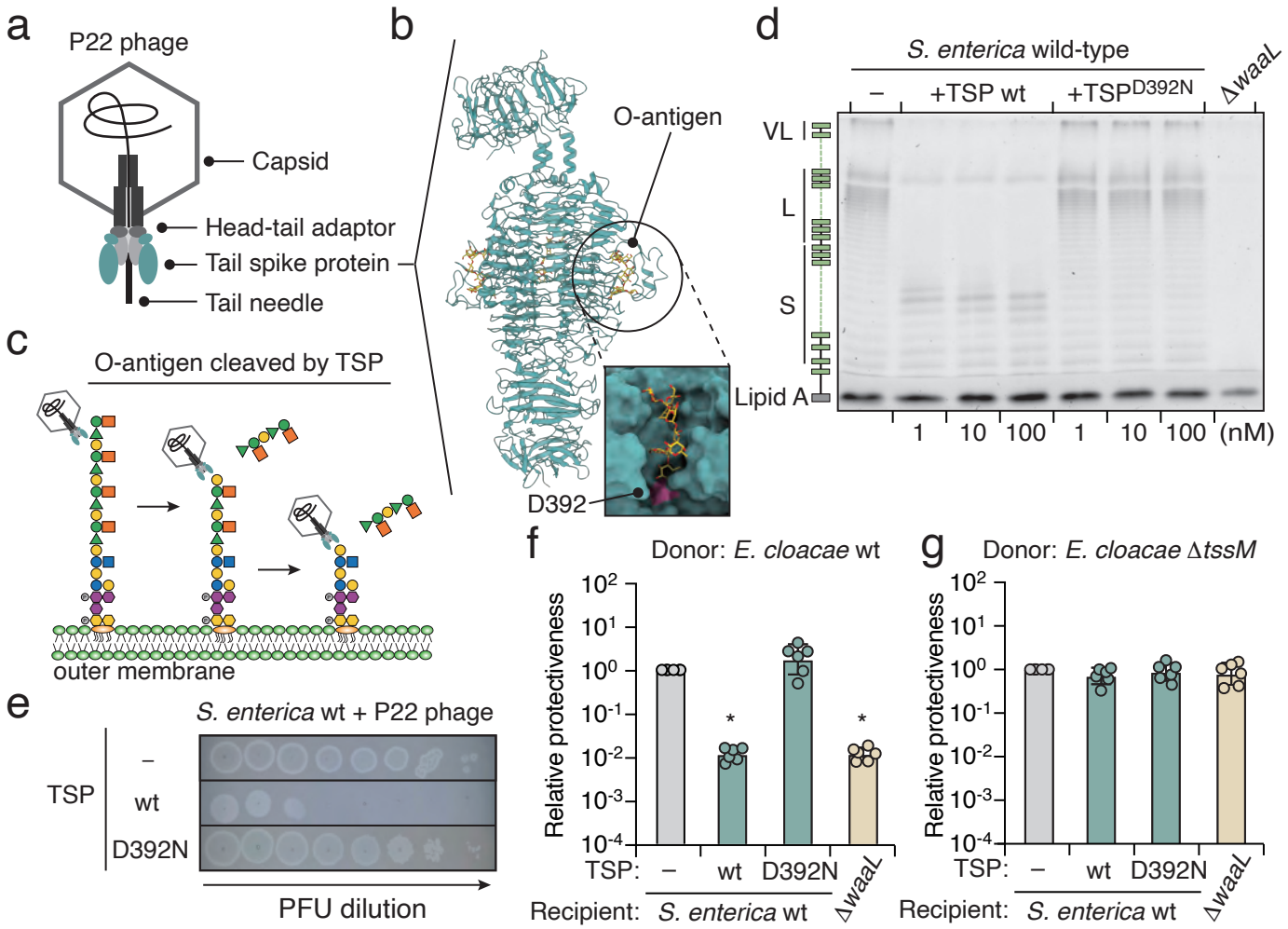
a
P22 phage
Capsid
Head-tail adaptor
Tail spike protein
Tail needle
b
O-antigen
D392
c
O-antigen cleaved by TSP
outer membrane
d
S. enterica wild-type
–
+TSP wt
+TSP D392N
ΔwaaL
VL
L
S
Lipid A
1
10
100
1
10
100
(nM)
e
S. enterica wt + P22 phage
TSP
–
wt
D392N
PFU dilution
f
Donor: E. cloacae wt
Relative protectiveness
TSP:
–
wt
D392N
ΔwaaL
Recipient:
S. enterica wt
g
Donor: E. cloacae ΔtssM
Relative protectiveness
TSP:
–
wt
D392N
ΔwaaL
Recipient:
S. enterica wt

Figure 5

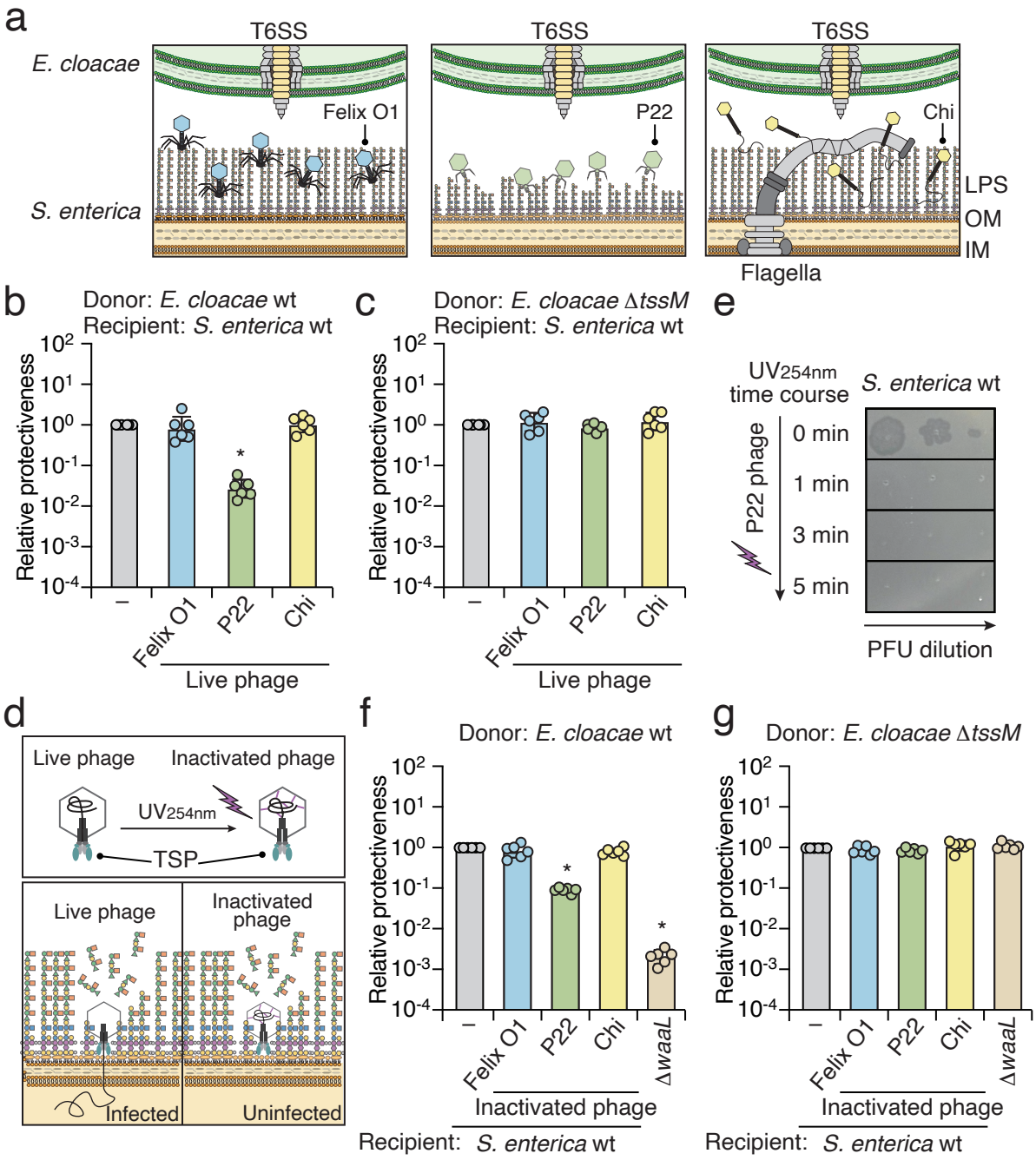
a
T6SS
E. cloacae
S. enterica
Felix O1
P22
Chi
LPS
OM
IM
Flagella
b
Donor: E. cloacae wt
Recipient: S. enterica wt
Relative protectiveness
–
Felix O1
P22
Chi
Live phage
c
Donor: E. cloacae ΔtssM
Recipient: S. enterica wt
e
UV254nm time course
S. enterica wt
P22 phage
0 min
1 min
3 min
5 min
PFU dilution
d
Live phage
Inactivated phage
UV254nm
TSP
Infected
Uninfected
f
Donor: E. cloacae wt
ΔwaaL
Inactivated phage
Recipient: S. enterica wt
g
Donor: E. cloacae ΔtssM

Figure 6

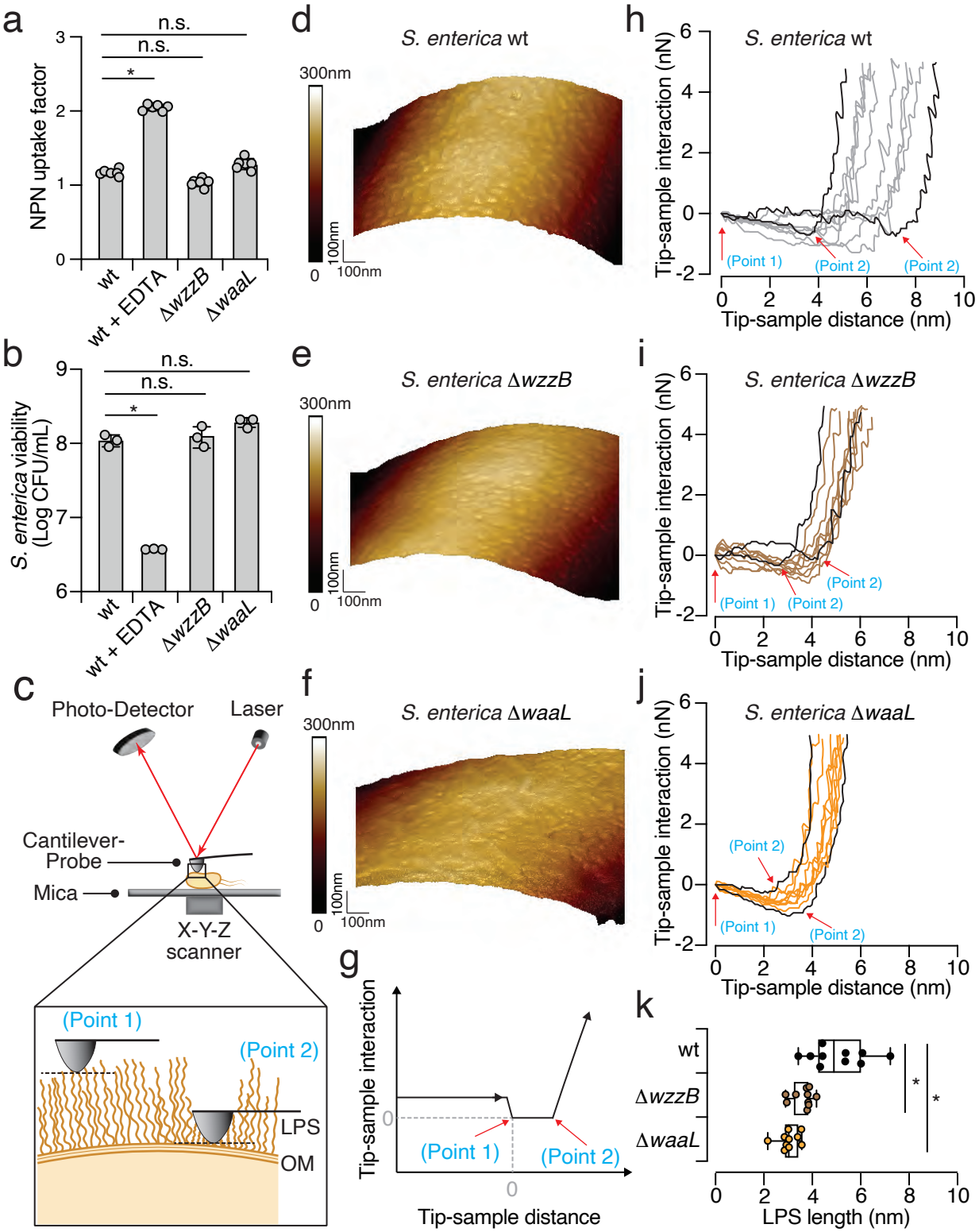
a
NPN uptake factor
n.s.
n.s.
*
wt
wt + EDTA
ΔwzzB
ΔwaaL
b
S. enterica viability (Log CFU/mL)
n.s.
n.s.
*
c
Photo-Detector
Laser
Cantilever-Probe
Mica
X-Y-Z scanner
(Point 1)
(Point 2)
LPS
OM
d
S. enterica wt
300nm
100nm
100nm
e
S. enterica ΔwzzB
f
S. enterica ΔwaaL
g
Tip-sample interaction
(Point 1)
(Point 2)
Tip-sample distance
h
S. enterica wt
Tip-sample interaction (nN)
Tip-sample distance (nm)
i
S. enterica ΔwzzB
j
S. enterica ΔwaaL
k
LPS length (nm)

Figure 7

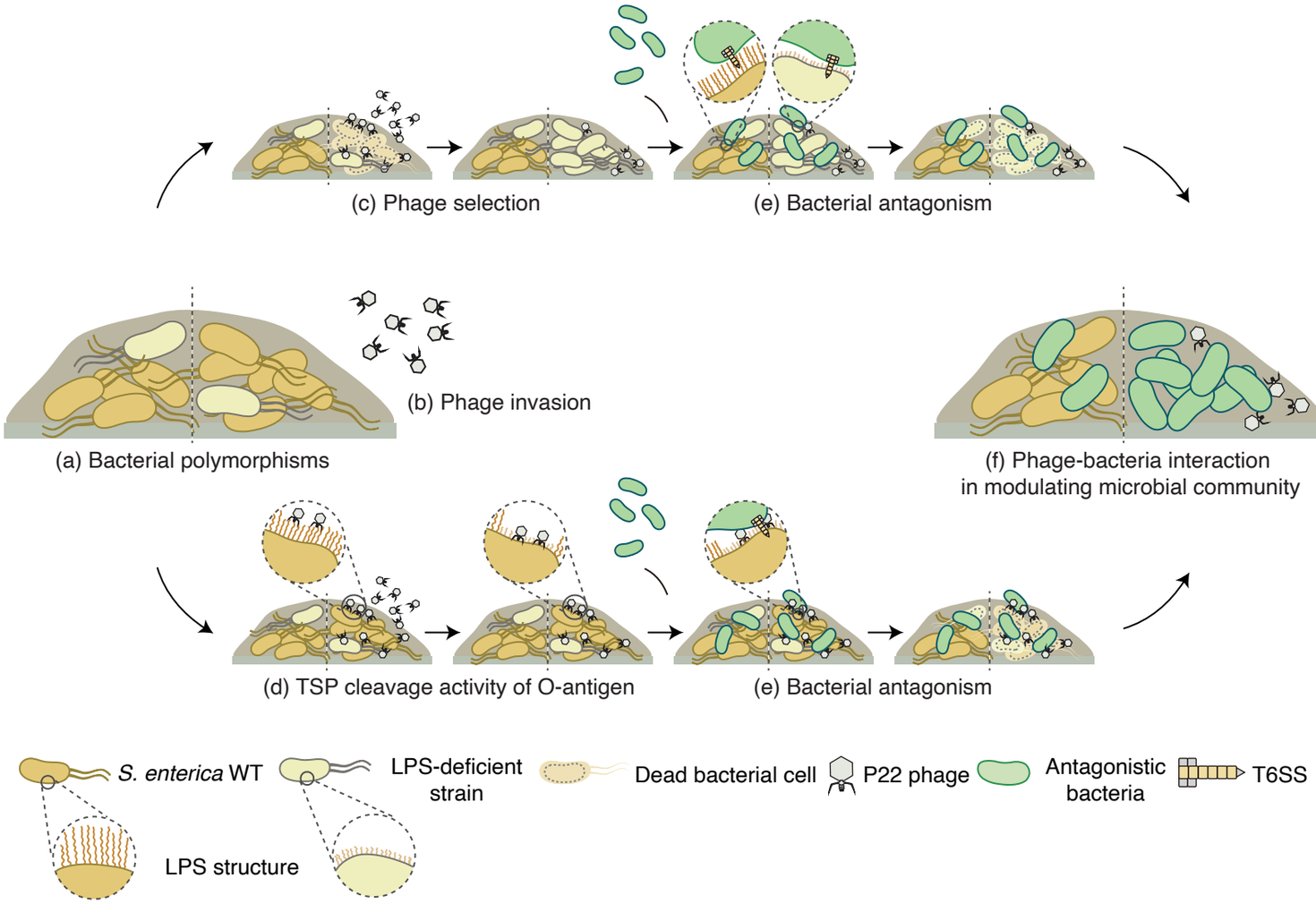
(c) Phage selection
(e) Bacterial antagonism
(a) Bacterial polymorphisms
(b) Phage invasion
(f) Phage-bacteria interaction
in modulating microbial community
(d) TSP cleavage activity of O-antigen
(e) Bacterial antagonism
S. enterica WT
LPS-deficient
strain
Dead bacterial cell
P22 phage
Antagonistic
bacteria
T6SS
LPS structure

Supplementary Figure 1

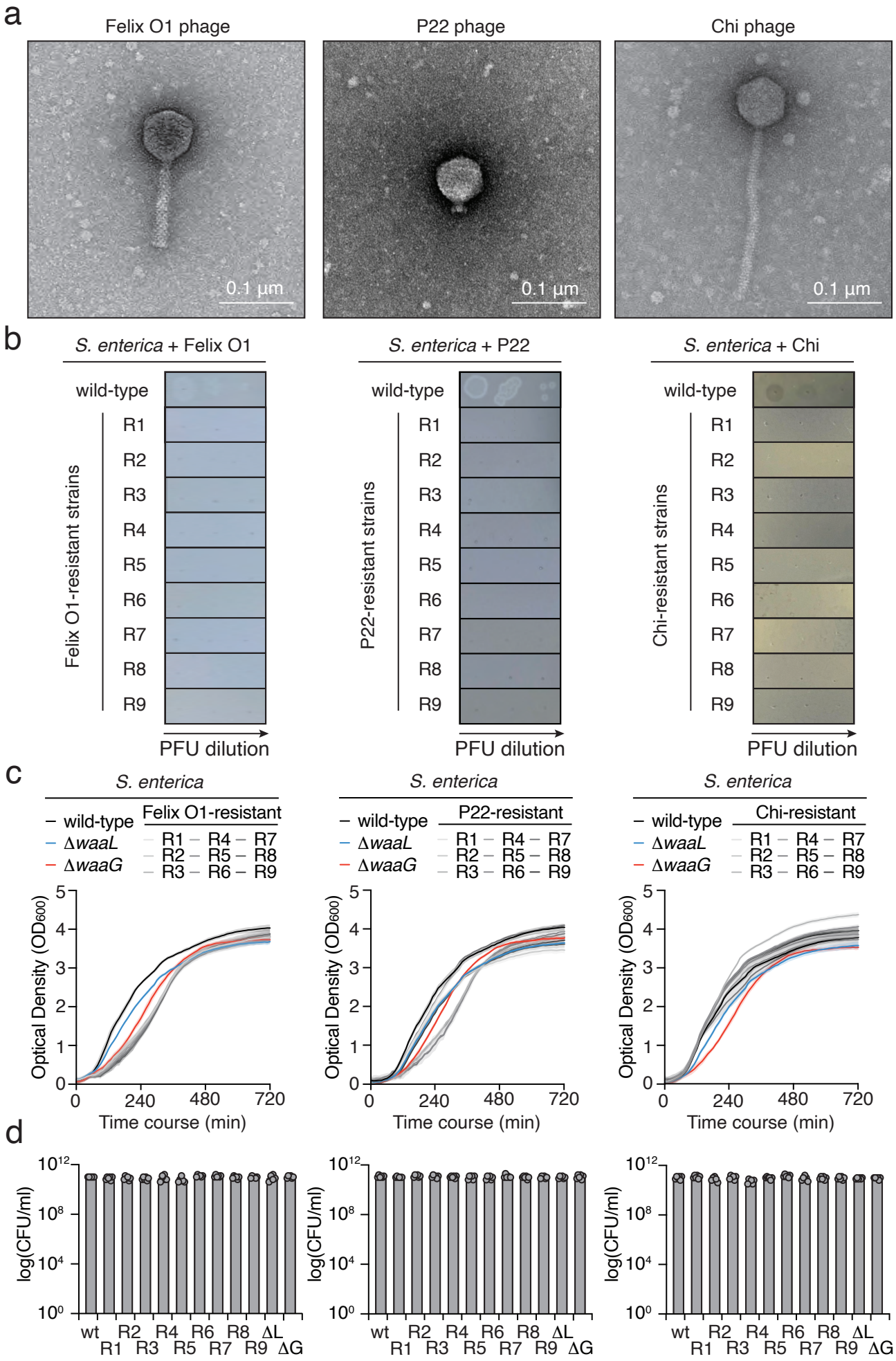

Supplementary Figure 2

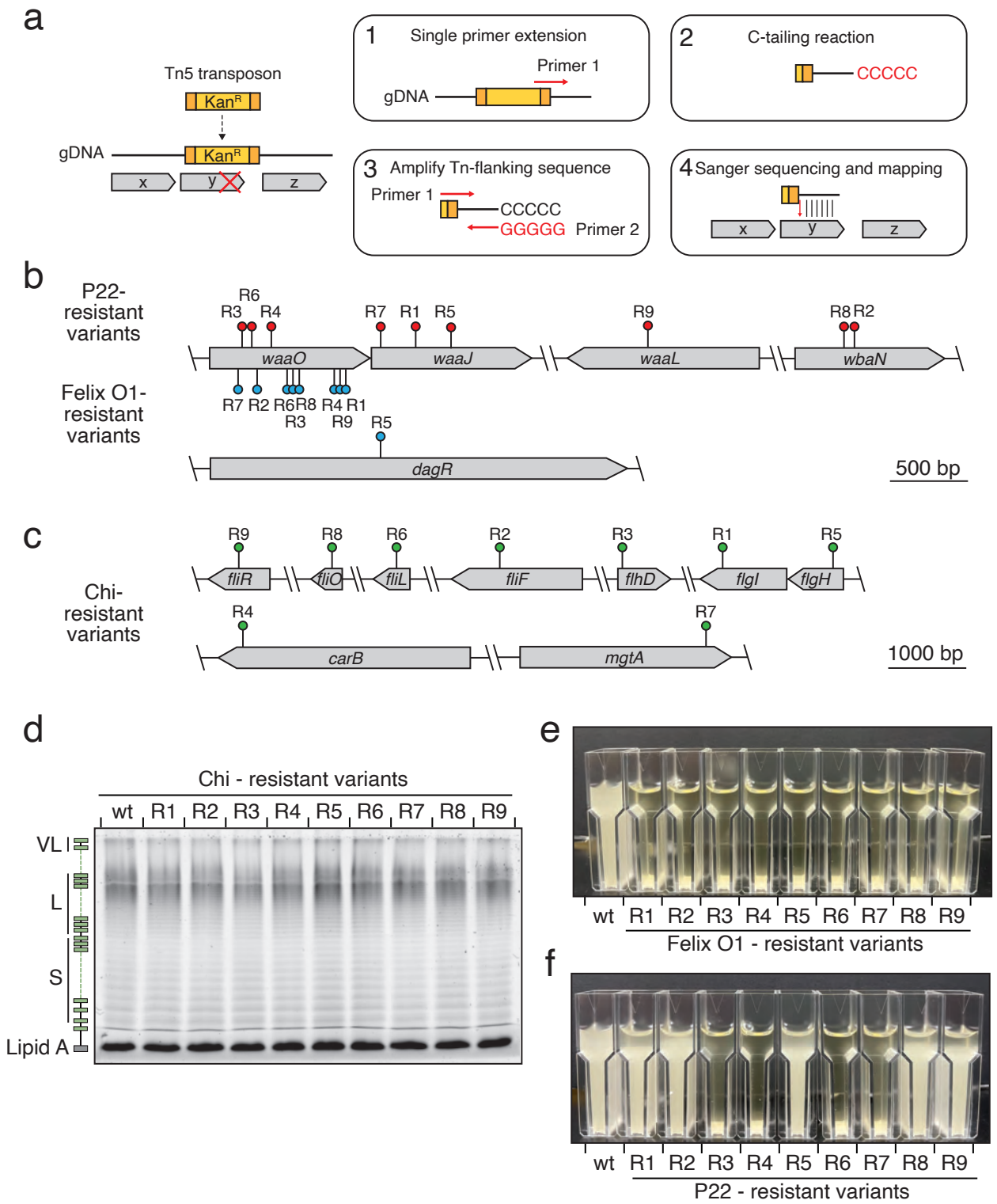

Supplementary Figure 3

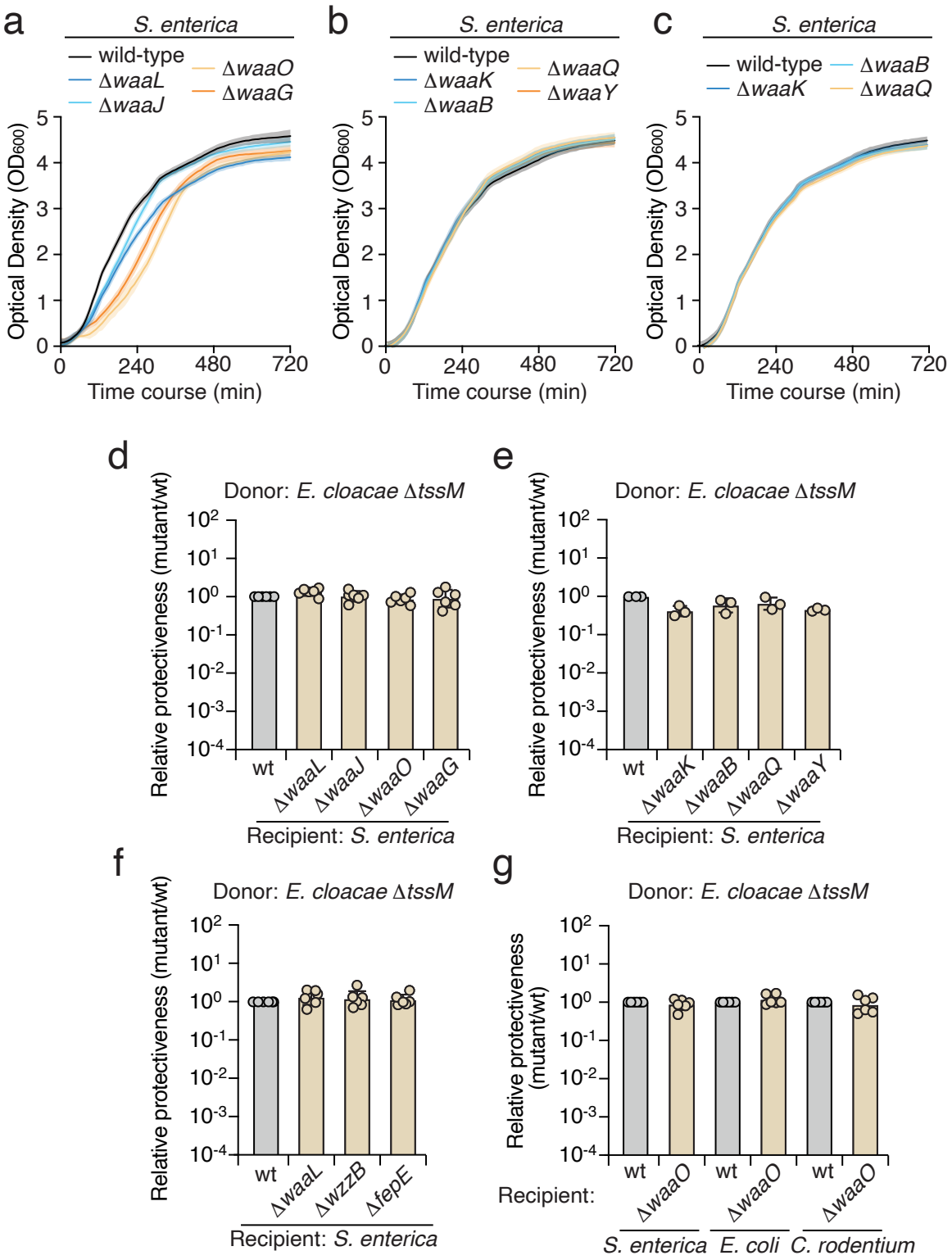

Supplementary Figure 4

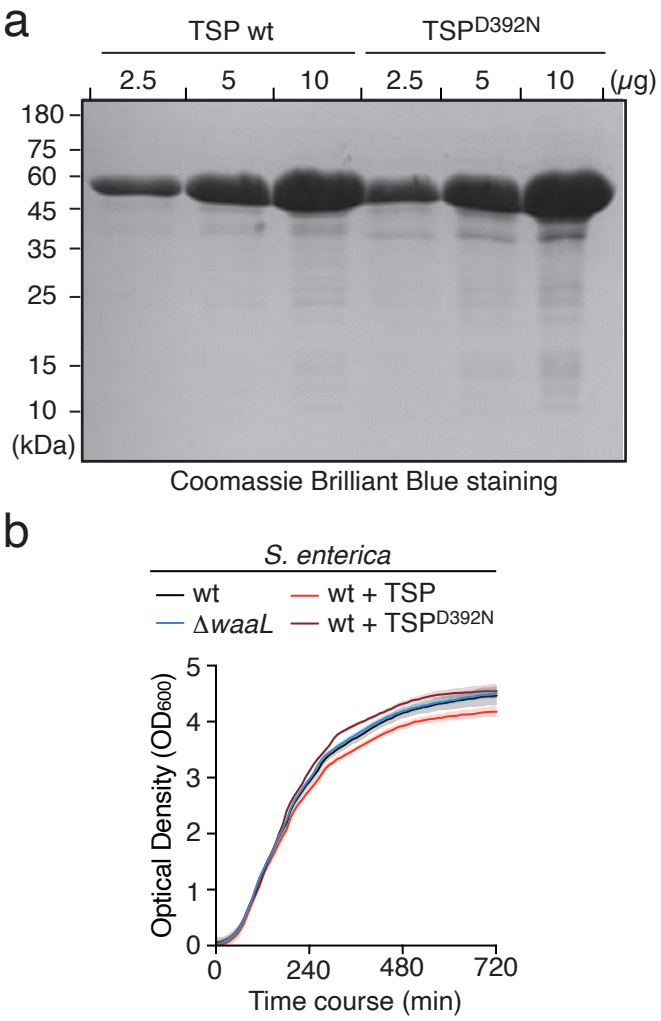

Supplementary Figure 5

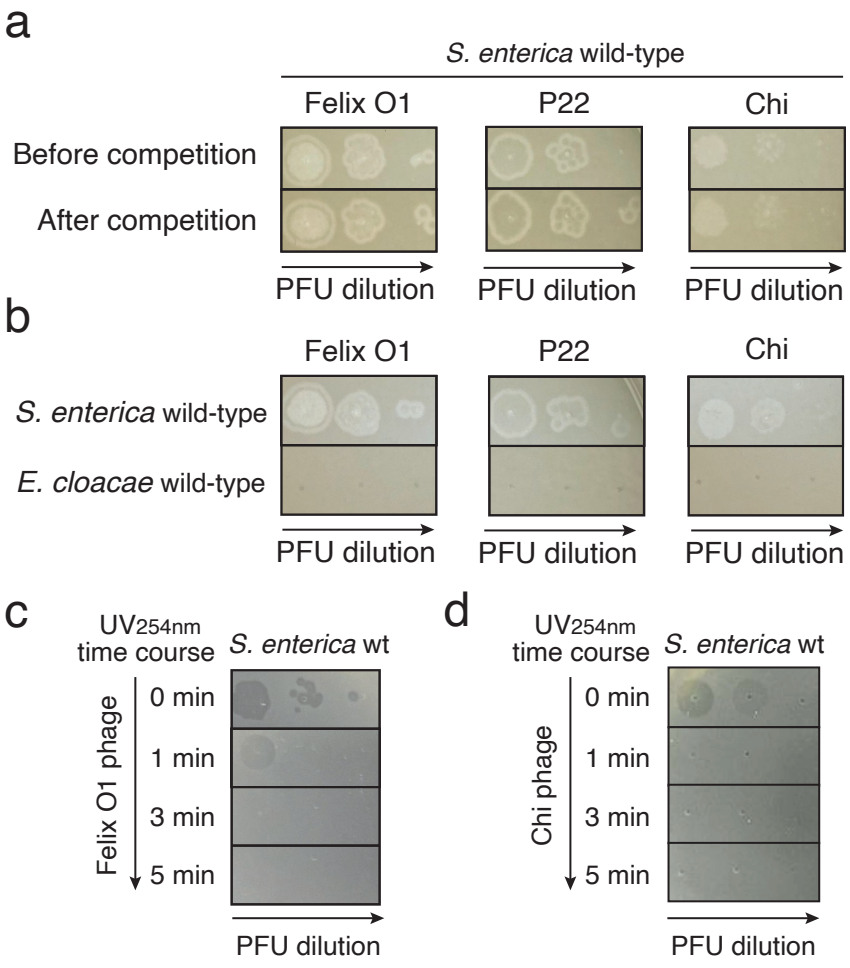

Supplementary Figure 6

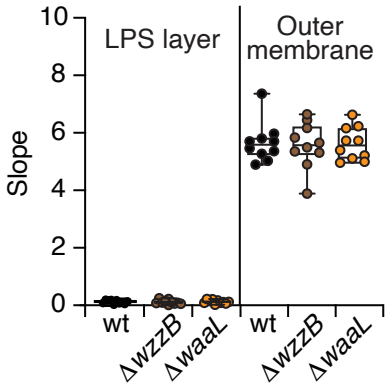

Supplementary Table 1. Strains, Recombinant DNA, and Oligonucleotides used in this study.

Strain	Source	Identifier
Escherichia coli DH5α	YB Biotech	Cat# XR-LYE678-80
Escherichia coli PIR1	Gift from Dr. Hsin-Hung David Chou	N/A
Escherichia coli BL21 pRIL (DE3)	Gift from Dr. Hung-Ta Chen	N/A
Escherichia coli S17-1 λ pir	Lab collection	N/A
Enterobacter cloacae	American Type Culture Collection	ATCC 13047
Enterobacter cloacae Δ*tssM*	Whitney et al., 2014	N/A
Enterobacter cloacae Δ*cdiA*	Beck et al., 2015	N/A
Salmonella enterica serovar Typhimurium	American Type Culture Collection	ATCC 14028
Salmonella enterica serovar Typhimurium Tn7::Chl	This paper	N/A
Salmonella enterica serovar Typhimurium LT2/(P22)+	Bioresource Collection and Research Center	BCRC 12459
Salmonella enterica bacteriophage Felix O1	Leibniz Institute DSMZ	DSM 18524
Salmonella enterica bacteriophage Chi	American Type Culture Collection	ATCC 9842-B1
Salmonella enterica serovar Typhimurium Tn7::Chl Δ*waaL*	This paper	N/A
Salmonella enterica serovar Typhimurium Tn7::Chl Δ*waaJ*	This paper	N/A
Salmonella enterica serovar Typhimurium Tn7::Chl Δ*waaO*	This paper	N/A
Salmonella enterica serovar Typhimurium Tn7::Chl Δ*waaG*	This paper	N/A
Salmonella enterica serovar Typhimurium Tn7::Chl Δ*waaK*	This paper	N/A
Salmonella enterica serovar Typhimurium Tn7::Chl Δ*waaB*	This paper	N/A
Salmonella enterica serovar Typhimurium Tn7::Chl Δ*waaQ*	This paper	N/A
Salmonella enterica serovar Typhimurium Tn7::Chl Δ*waaY*	This paper	N/A
Salmonella enterica serovar Typhimurium Tn7::Chl Δ*wzzB*	This paper	N/A
Salmonella enterica serovar Typhimurium Tn7::Chl Δ*fepE*	This paper	N/A
Enterohemorrhagic *Escherichia coli* O157:H7 EDL933	American Type Culture Collection	ATCC-43895

Enterohemorrhagic *Escherichia coli* O157:H7 EDL933 Tn7::Chl	This paper	N/A
Enterohemorrhagic *Escherichia coli* O157:H7 EDL933 Tn7::Chl Δ*waaO*	This paper	N/A
Citrobacter rodentium DBS100	American Type Culture Collection	ATCC-51459
Citrobacter rodentium DBS100 Δ*waaO*	This paper	N/A
Felix O1-resistant *Salmonella enterica* serovar Typhimurium-R1	This paper	N/A
Felix O1-resistant *Salmonella enterica* serovar Typhimurium-R2	This paper	N/A
Felix O1-resistant *Salmonella enterica* serovar Typhimurium-R3	This paper	N/A
Felix O1-resistant *Salmonella enterica* serovar Typhimurium-R4	This paper	N/A
Felix O1-resistant *Salmonella enterica* serovar Typhimurium-R5	This paper	N/A
Felix O1-resistant *Salmonella enterica* serovar Typhimurium-R6	This paper	N/A
Felix O1-resistant *Salmonella enterica* serovar Typhimurium-R7	This paper	N/A
Felix O1-resistant *Salmonella enterica* serovar Typhimurium-R8	This paper	N/A
Felix O1-resistant *Salmonella enterica* serovar Typhimurium-R9	This paper	N/A
P22-resistant *Salmonella enterica* serovar Typhimurium-R1	This paper	N/A
P22-resistant *Salmonella enterica* serovar Typhimurium-R2	This paper	N/A
P22-resistant *Salmonella enterica* serovar Typhimurium-R3	This paper	N/A
P22-resistant *Salmonella enterica* serovar Typhimurium-R4	This paper	N/A
P22-resistant *Salmonella enterica* serovar Typhimurium-R5	This paper	N/A
P22-resistant *Salmonella enterica* serovar Typhimurium-R6	This paper	N/A
P22-resistant *Salmonella enterica* serovar Typhimurium-R7	This paper	N/A
P22-resistant *Salmonella enterica* serovar Typhimurium-R8	This paper	N/A
P22-resistant *Salmonella enterica* serovar Typhimurium-R9	This paper	N/A

Chi-resistant *Salmonella enterica* serovar Typhimurium-R1	This paper	N/A
Chi-resistant *Salmonella enterica* serovar Typhimurium-R2	This paper	N/A
Chi-resistant *Salmonella enterica* serovar Typhimurium-R3	This paper	N/A
Chi-resistant *Salmonella enterica* serovar Typhimurium-R4	This paper	N/A
Chi-resistant *Salmonella enterica* serovar Typhimurium-R5	This paper	N/A
Chi-resistant *Salmonella enterica* serovar Typhimurium-R6	This paper	N/A
Chi-resistant *Salmonella enterica* serovar Typhimurium-R7	This paper	N/A
Chi-resistant *Salmonella enterica* serovar Typhimurium-R8	This paper	N/A
Chi-resistant *Salmonella enterica* serovar Typhimurium-R9	This paper	N/A

Recombinant DNA	**Source**
pRE118_SentΔ*waaL*	This paper
pRE118_SentΔ*waaJ*	This paper
pRE118_SentΔ*waaO*	This paper
pRE118_SentΔ*waaG*	This paper
pRE118_SentΔ*waaK*	This paper
pRE118_SentΔ*waaB*	This paper
pRE118_SentΔ*waaQ*	This paper
pRE118_SentΔ*waaY*	This paper
pRE118_SentΔ*wzzB*	This paper
pRE118_SentΔ*fepE*	This paper
pRE118_EcoliΔ*waaO*	This paper
pRE118_CrodΔ*waaO*	This paper
pETDuet-1-His6_P22TSP	This paper
pETDuet-1-His6_P22TSP D392N	This paper
pGRG37	McKenzie et al. 2006

Primer	**Sequences (5'-3')**	**Identifier**
Bacteria strain construction		
Sent_ΔwaaL_F1	CATGAATTCCCGGGAGAGCTCATCAAAGCGGAACGCACAG	Mission Biotech
Sent_ΔwaaL_R1	TTTATCTATTGGTTAGCATCTTTTCTCCACAATAG	Mission Biotech
Sent_ΔwaaL_F2	GATGCTAACCAATAGATAAAAAAACGCGC	Mission Biotech

Sent_ΔwaaL_R2	CGACGGATCCCAAGCTTCTTCTAGAACCAGAACTTCCTGATAATG	Mission Biotech
Sent_ΔwaaL_seq_F	TGATTCCCGTCGCTATTCGC	Mission Biotech
Sent_ΔwaaL_seq_R	AGATCAGAGAGCGCAATCCG	Mission Biotech
Sent_ΔwaaJ_F1	CATGAATTCCCGGGAGAGCTCGTACGCTACGCAGATTGTTG	Mission Biotech
Sent_ΔwaaJ_R1	ATTATTTGTGTGAATCCATTACATCACCTATG	Mission Biotech
Sent_ΔwaaJ_F2	AATGGATTCACACAAATAATTCCCCTCC	Mission Biotech
Sent_ΔwaaJ_R2	CGACGGATCCCAAGCTTCTTCTAGACCTTACCCTTAATACGAC	Mission Biotech
Sent_ΔwaaJ_seq_F	TGAAGACCAGCAGCGATTTG	Mission Biotech
Sent_ΔwaaJ_seq_R	ACGTGCTACATTGATCAGCG	Mission Biotech
Sent_ΔwaaO_F1	CATGAATTCCCGGGAGAGCTCGTGATATGTATTGATGTCATCTC	Mission Biotech
Sent_ΔwaaO_R1	TTTATTCAAGTCTGCTCATAGTGATCAC	Mission Biotech
Sent_ΔwaaO_F2	TATGAGCAGACTTGAATAAAACCCATAGGTG	Mission Biotech
Sent_ΔwaaO_R2	CGACGGATCCCAAGCTTCTTCTAGAGTGACTTATCTTTCAACTCAC	Mission Biotech
Sent_ΔwaaO_seq_F	CTTCGTCGAGCTAAGCATG	Mission Biotech
Sent_ΔwaaO_seq_R	TGTAGCGCCCGTATAATG	Mission Biotech
Sent_ΔwaaG_F1	CATGAATTCCCGGGAGAGCTCAATCTCACCGATCAGTGG	Mission Biotech
Sent_ΔwaaG_R1	CTCAACCATCAACTCTCATAGCAGGCTG	Mission Biotech
Sent_ΔwaaG_F2	TATGAGAGTTGATGGTTGAGCTGAAAGC	Mission Biotech
Sent_ΔwaaG_R2	CGACGGATCCCAAGCTTCTTCTAGACACTCATAAATTACTCACTGAG	Mission Biotech
Sent_ΔwaaG_seq_F	AGATCAAAAACGCGCTATCG	Mission Biotech
Sent_ΔwaaG_seq_R	GCAATGTCCAGTCTTCTTCC	Mission Biotech
Sent_ΔwaaK_F1	CATGAATTCCCGGGAGAGCTCAAGATGTCATTGCAGTCAATG	Mission Biotech
Sent_ΔwaaK_R1	ATCACTTATCTTTAATCATAATAGCTATAATCCAGAATAG	Mission Biotech
Sent_ΔwaaK_F2	TATGATTAAAGATAAGTGATTGAGTCCTG	Mission Biotech

Sent_ΔwaaK_R2	CGACGGATCCCAAGCTTCTTCTAGACATCGACATATGTCCGATTC	Mission Biotech
Sent_ΔwaaK_seq_F	GGTCCTACGTCCAGAAAGAC	Mission Biotech
Sent_ΔwaaK_seq_R	TTTAGGACTTCGCTGCCTTG	Mission Biotech
Sent_ΔwaaB_F1	CATGAATTCCCGGGAGAGCTCGAAGACTACTGTGCTGAC	Mission Biotech
Sent_ΔwaaB_R1	ATCACTTTTGTATTTTCATATATACCCCAGAG	Mission Biotech
Sent_ΔwaaB_F2	TATGAAAATACAAAAGTGATCACTATGAGC	Mission Biotech
Sent_ΔwaaB_R2	CGACGGATCCCAAGCTTCTTCTAGATACAGTCTCAGCATCAAC	Mission Biotech
Sent_ΔwaaB_seq_F	TGGGCGTTGATACGATGCAC	Mission Biotech
Sent_ΔwaaB_seq_R	ACTATGCCAGGGCTTCGTTG	Mission Biotech
Sent_ΔwaaQ_F1	CATGAATTCCCGGGAGAGCTCGTGCAGCGCAGCAATCAG	Mission Biotech
Sent_ΔwaaQ_R1	CTCATAGCAGCTTTTCCACAAGCGACTCTTTG	Mission Biotech
Sent_ΔwaaQ_F2	TGTGGAAAAGCTGCTATGAGAGTTGCCTTTTG	Mission Biotech
Sent_ΔwaaQ_R2	CGACGGATCCCAAGCTTCTTCTAGACCATTAACTCCGCGATATC	Mission Biotech
Sent_ΔwaaQ_seq_F	GCGCATTAGCGATAACCAGG	Mission Biotech
Sent_ΔwaaQ_seq_R	CCTGATAGGCTGGATGCAG	Mission Biotech
Sent_ΔwaaY_F1	for making Salmonella 14028 ChlR waaY/rfaY (EJJ31_RS00655) deletion with pRE118	Mission Biotech
Sent_ΔwaaY_R1	ATCAGCGTTTAATAATCATAATGGAGATTTAGGG	Mission Biotech
Sent_ΔwaaY_F2	TATGATTATTAAACGCTGATCAATGTAG	Mission Biotech
Sent_ΔwaaY_R2	CGACGGATCCCAAGCTTCTTCTAGAATTCGTCATAGAAACGTG	Mission Biotech
Sent_ΔwaaY_seq_F	GTTTAGCCGTACAGCATCAC	Mission Biotech
Sent_ΔwaaY_seq_R	TAAGCTCAGATGGCATAGGG	Mission Biotech
Sent_ΔwzzB_F1	CATGAATTCCCGGGAGAGCTCACTCCAGGAAGGCGCTATTAAAC	Mission Biotech
Sent_ΔwzzB_R1	CTTACAAGGCCACTGTCATAGATACCCTAACTAAAAAAAGGATG	Mission Biotech

Sent_ΔwzzB_F2	TATGACAGTGGCCTTGTAAGCTTCTTTGCCGGATG	Mission Biotech
Sent_ΔwzzB_R2	CGACGGATCCCAAGCTTCTTCTAGATGTCGACGGCGCGC	Mission Biotech
Sent_ΔwzzB_seq_F	CGTGATTGGGGAACAGTCTG	Mission Biotech
Sent_ΔwzzB_seq_R	CTTGAGGCATTCCGTGATGC	Mission Biotech
Sent_ΔfepE_F1	CATGAATTCCCGGGAGAGCTCCTATACCGTCGCAAAAAACC	Mission Biotech
Sent_ΔfepE_R1	CATGCCATCTTTAGTCTGATTTACCCGAAAAGC	Mission Biotech
Sent_ΔfepE_F2	ATCAGACTAAAGATGGCATGCCGTATGAC	Mission Biotech
Sent_ΔfepE_R2	CGACGGATCCCAAGCTTCTTCTAGAAGGTATGTGAACATCATC	Mission Biotech
Sent_ΔfepE_seq_F	CCTATGCAAACCGCAACCACCC	Mission Biotech
Sent_ΔfepE_seq_R	CCGAATCCGTAGCCCGTTTGC	Mission Biotech
Ecoli_ΔwaaO_F1	CATGAATTCCCGGGAGAGCTCCGTTATGGCGCGGTAAAG	Mission Biotech
Ecoli_ΔwaaO_R1	TTTAGAAGCATTGAGACATATTTATTCTGTATCCAAAATTTTG	Mission Biotech
Ecoli_ΔwaaO_F2	TATGTCTCAATGCTTCTAAAGATTTAAGGTTAAAATAATTC	Mission Biotech
Ecoli_ΔwaaO_R2	CGACGGATCCCAAGCTTCTTCTAGAGCGCTTGTCCAGTTCAATTATATC	Mission Biotech
Ecoli_ΔwaaO_seq_F	GATGGTTGAACTTAAAGAGCCG	Mission Biotech
Ecoli_ΔwaaO_seq_R	CCTGGTAGTTCTCATCAATACC	Mission Biotech
Crod_ΔwaaO_F1	CATGAATTCCCGGGAGAGCTCCGTTATGGCGCGGTAAAG	Mission Biotech
Crod_ΔwaaO_R1	TTTAGAAGCATTGAGACATATTTATTCTGTATCCAAAATTTTG	Mission Biotech
Crod_ΔwaaO_F2	TATGTCTCAATGCTTCTAAAGATTTAAGGTTAAAATAATTC	Mission Biotech
Crod_ΔwaaO_R2	CGACGGATCCCAAGCTTCTTCTAGAGCGCTTGTCCAGTTCAATTATATC	Mission Biotech
Crod_ΔwaaO_seq_F	ATTAATGCATTTAGCCAGTGGC	Mission Biotech
Crod_ΔwaaO_seq_R	TGTATCTTCTGAAATTATGCGC	Mission Biotech

Plasmid construction		
pETDuet_TSP_F	ACCATCATCACCACAGCCAGGATCCAGATCAATATTCAATAGAAGC	Mission Biotech
pETDuet_TSP_R	GTTCGACTTAAGCATTATGCGGCCGCTAAAGTGTTGCCAAGGTTAATCTAACTAATTC	Mission Biotech
pETDuet_TSP_D392N_F	CCCCGTATGGAATGGATTCGATTTAGGTGCTGAC	Mission Biotech
pETDuet_TSP_D392N_R	CGAATCCATTCCATACGGGGTAAATAACGACC	Mission Biotech
pETDuet_Seq_F	ATGCGTCCGGCGTAGA	Mission Biotech
pETDuet_Seq_R	GATTATGCGGCCGTGTACAA	Mission Biotech
pRE118_seq_F	GGTTGAGAAGCGGTGTAAGTG	Mission Biotech
pRE118_seq_R	GCAGGTCGATCCCAAGCTTC	Mission Biotech
Transposon Insertion mapping		
EzTn5_s	GATCCTCTAGAGTCGACCTGCAGGCATGCA	Integrated DNA Technologies, Inc.
Tn5_F	TCGTCGGCAGCGTCAGATGTGTATAAGAGACAG	Integrated DNA Technologies, Inc.
Tn5_R	GTCTCGTGGGCTCGGAGATGTGTATAAGAGACAGGGGGGGGGGGGGGGG	Integrated DNA Technologies, Inc.